Developing a model system for studying the ozone processing of atmospheric aerosols by following changes in surface properties

Erick González – Labrada

A Thesis

in

The Department

of

Chemistry and Biochemistry

Presented in Partial Fulfillment of the Requirements
for the Degree of Doctor of Philosophy at
Concordia University
Montréal, Québec, Canada

August 2007

Your file Votre référence
ISBN: 978-0-494-31115-8
Our file Notre référence
ISBN: 978-0-494-31115-8

ABSTRACT

Developing a model system for studying the ozone processing of atmospheric aerosols by following changes in surface properties

Erick González – Labrada, Ph.D.
Concordia University, 2007

Atmospheric aerosols have a significant organic composition as determined by field measurement studies. This organic material is released to the atmosphere from both natural and anthropogenic sources, such as wind bursting of the ocean surface, car exhausts, and meat cooking, among others. An inverted micelle model has been proposed in order to explain the high concentration of organic compounds in aerosol particles. The model describes an organic film coating the air-liquid interface of an aqueous aerosol core.

Chemical processing of this organic film by atmospheric oxidants (such as OH radicals, O_3, and NO_3) through heterogeneous and multiphase reactions can activate the aerosol to participate in atmospheric chemistry. After reaction, the particle has an increased role in the absorption and scattering of incoming solar radiation and cloud formation. Another consequence of this oxidation is the decrease of the atmospheric budget of gas-phase trace species, as well as the formation of volatile products.

Several studies have proposed that the ozonolysis of organic films in aerosols takes place mainly at the surface. Therefore, the objective of this research was to develop a suitable model system for following the reaction through quantitative changes of a property inherent to the surface. Several attempts were made to examine the ozonolysis of organic monolayers at either solid or liquid surfaces. The studied monolayers contained unsaturated organic compounds as the only component or as part of a binary mixture with saturated compounds.

The study of the ozone processing of monolayers deposited on solid substrates revealed information about changes in the hydrophobic character of the surface that occurred because of the reaction. On the other hand, the processing of a monolayer spread on a pendant drop allowed a real-time monitoring of surface pressure changes. This permitted a kinetic study of the reaction that yielded parameters related exclusively to processes taking place at the surface. For instance, the measured reactive uptake coefficient of ozone γ_{meas} was estimated to be $(2.6 \pm 0.1) \times 10^{-6}$. The versatility offered by the latter system to the study of heterogeneous chemical reactions taking place at the air-liquid interface is explained as well as possible future directions for its utilization are given.

ACKNOWLEDGEMENTS

Finishing this thesis project would have not been possible without the support of several people during these four years at Concordia University.

First, I would like to thank my supervisor Dr. Christine DeWolf for introducing me to a challenging research project that interested me and that I enjoyed working on. I especially thank her for always being available to discuss my results, doubts or ideas. I also highly appreciate that she attended my thesis defense (special thanks to Erik Aleksander, for behaving so well during those two hours). In addition, thanks to her passion for soccer, I was able to enjoy playing several good matches with department people, and felt supported when postponing an experiment due to a crucial soccer game.

I thank Dr. Rolf Schmidt for helpful answers to problems and doubts, for showing me the importance of organizing my research, and for those fantastic illustrations. I would like to thank the members of my committee, Dr. Louis Cuccia, and Dr. Yves Gélinas, for contributing their opinions and comments about my work, as well as the external examiners, Dr. James Donaldson and Dr. Catherine Mulligan for their useful comments on this manuscript.

Thanks to current and past members of Dr. DeWolf's research group for their suggestions, help and company, particularly the undergraduate students who participated in this research project. Thanks to the workshop staff who was always enthusiastic to work on any idea of experimental setup. In addition, I am grateful to everyone – professors, staff, and students – at the department of Chemistry and Biochemistry, which has always been a comfortable and friendly environment.

Many people did not directly contribute nor were directly involved in my research project, however, they made my time in Montreal more enjoyable, and I thank all my friends here for those moments. I am especially grateful to Ernesto for sharing these four years and the eventful months of thesis writing.

Thanks to my closest friends for being always near in spite of time and distance.

Thanks to Einat, for her love, care, and patience, and for enduring together the difficulties of finishing this thesis.

And finally, thanks to my family, Mima, Pipo, Gordis y Grazi, for defining who I am and for making this journey that started almost seven years ago, meaningful. Ustedes más que nadie han esperado por este momento. Esta tesis es para ustedes.

TABLE OF CONTENTS

LIST OF FIGURES

LIST OF TABLES

LIST OF SYMBOLS

A	area per mole of a compound at the surface
a	the radius of an aerosol particle
$\bar{c}$	mean kinetic speed of ozone molecules in the gas phase
D_g	diffusion of the gas
D_l	gas diffusion in the liquid bulk
H	Henry's law constant
Kn	Knudsen number
k'	pseudo-first order rate constant
k_{des}	rate of desorption from the surface
k_{solv}	rate of entrance to the bulk liquid
n_0	bulk concentration of ozone
R	ideal gas constant
S	probability of adsorption or accommodation at the surface
T	temperature
α	mass accommodation coefficient
Γ_{diff}	resistance term representing gas diffusion
Γ_g	resistance term representing the transport of gas species to the particle surface
Γ_{rxn}	resistance term representing the reaction in the bulk
Γ_{surf}	resistance term representing the reaction at the surface
γ	surface tension measured when a monolayer is present on the surface
γ_0	surface tension of pure water
γ_{meas}	measured uptake probability of a gas by a particle
γ_{net}	net uptake probability of a gas by a particle
$\Delta\theta$	variation of the contact angle with the exposure
δ	thickness of the surface layer
λ	mean free path of the gas
θ_I	contact angle values before exposure
θ_F	contact angle values after exposure
π	surface pressure
σ	standard deviation

LIST OF ABBREVIATIONS

ADSA	axisymmetric drop shape analysis
AFM	atomic force microscopy
ATR-FTIR	attenuated total reflection infrared spectroscopy
BBSFG	broad-bandwidth, sum frequency generation spectroscopy
CCN	cloud condensation nuclei
DMPC	1,2-dimyristoyl-*sn*-glycero-3-phosphocholine
DOPC	1,2-dioleoyl-*sn*-glycero-3-phosphocholine
DPPC	1,2-dipalmitoyl-*sn*-glycero-3-phosphocholine
DSPC	1,2-distearoyl-*sn*-glycero-3-phosphocholine
GC-MS	gas chromatography-mass spectrometry
IRRAS	infrared reflection absorption spectroscopy
OPPC	1-oleoyl-2-palmitoyl-*sn*-glycero-3-phosphocholine
PAH	polycyclic aromatic hydrocarbon
SAM	self-assembled monolayer
TFM	transmission force microscopy

Chapter 1

INTRODUCTION

1.1. Atmosphere, ozone, and atmospheric aerosols

The atmosphere consists of layers of gases surrounding our planet in which temperature varies with altitude and chemical composition is diverse. The atmosphere contributes to the development of life by absorbing harmful ultraviolet solar radiation and balancing the planet temperature. The more important atmospheric layers for the protection of life are the troposphere and the stratosphere, the two closest to the ground in that order.

The troposphere extends to 10-15 km from the ground, depending on the location on the planet. In this layer the temperature decreases with increasing altitude from an average 15°C on the ground to approximately -55°C, as the heating effect of the surface due to absorbed radiation diminishes. In the boundary region between troposphere and stratosphere, temperatures start rising again with altitude because of the presence of the ozone layer in the stratosphere, and therefore, the occurrence of photochemical reactions involving ozone and molecular oxygen. The top of the stratosphere is found around 50 km above ground, where the temperature could reach values up to -3°C.

Ozone (O_3) is an allotrope of oxygen, a triatomic molecule that is less stable than the diatomic species. It is a gas at standard temperature and pressure, and a powerful oxidizing agent. The stratospheric ozone is essential for life as it absorbs ultraviolet light of $\lambda < 290$ nm, which is recognized as a biologically harmful radiation. The ozone layer is found in a region of 15 to 35 km above the ground with concentrations between 2 to 10 ppm[1], although both layer thickness and concentration change between different geographical locations and seasons. Ozone is also found in the troposphere as the product of photochemical reactions initiated by precursors of mainly anthropogenic origin such as volatile organic compounds and nitrogen oxides[2]. Normal concentrations are found to be lower than 0.2 ppm, with higher ozone levels being considered serious air pollution episodes and highly prejudicial to human health[2]. At concentrations found in the troposphere, ozone is already considered an important atmospheric oxidant with the potential to participate in several reactions like those occurring in the condensed phase involving aerosol particles.

Aerosols are ubiquitous in the atmosphere as suspensions of solid and liquid particles in a gaseous environment. Their presence is observed in big cities during smog episodes or as fog and mist either in inhabited or in unpopulated areas. However, their influence on climate goes far beyond what everyday is observed. As they absorb and scatter incoming solar radiation, aerosols have a significant impact on the temperature of the planet. Global and local climate can be affected by their role in cloud formation, and subsequently, cloud lifetime and precipitation. In addition, aerosol particles have been linked to the incidence of respiratory diseases and impaired visibility in polluted areas[3].

Among their characteristics, the particle size distribution is of considerable importance since it is the primary determining factor in the incidence of respiratory illnesses. For instance, the number of aerosol particles in the troposphere can be found in the range of 10^2-10^5 cm^{-3}, with mass concentrations of 1-100 $\mu g\ m^{-3}$, which shows how variable their number and spatial distribution can be[4]. On the other hand, the composition of atmospheric aerosols is wide and complex, and directly related to the particle origin and fate. Recent reports estimate that the contribution of organic material to the total fine aerosol mass is ~20-50% in continental regions and up to 90% in tropical areas[5]. A significant fraction of the organic composition of atmospheric particles is made up of water-soluble compounds[5], but other hydrophobic organic compounds are also common. For instance, a field measurement of a marine aerosol episode measured concentrations for known fatty acids like palmitic acid, stearic acid, oleic acid, and linoleic acid of 5.3 (principal component of this aerosol mass), 2.4, 1.7, and 3.1 $ng\ m^{-3}$, respectively[6].

In general, this organic material has been identified to contain compounds of either biogenic or anthropogenic origin such as aliphatic hydrocarbons, carboxylic acids, amines and other organic bases, polycyclic aromatic hydrocarbons, and other aromatic polar compounds, together with water, inorganic acids, and salts like sulfates and nitrates. The organic composition can play an important role by accentuating the effect of aerosols on global climate, participating in heterogeneous chemical reactions and multiphase processes, or as a means of transportation for pollutant molecules throughout the atmosphere and to remote locations[1,6]. Recently, research has focused on the study of atmospheric aerosols as promoters of the evolution of life on earth[7]. The surface of

aerosols could have been the scenery of condensation of small gases, and formation of the first hydrocarbons and amino acids, through reactions taking place in similar ways as today.

Accurate models of the chemical balance of the atmosphere have been built from what is known about reactions occurring in the homogeneous gas phase[3]. Although they have permitted to predict and forecast climate changes, they have occasionally failed, as they do not completely include the effects of atmospheric aerosols on the climate (e.g. acid rains)[3]. Research on heterogeneous reactions taking place in the condensed phase has shown rates fast enough to compete with gas phase reactions. Several atmospheric oxidants, such as OH radicals, O_3, and NO_3, can react with aerosol-based organic compounds through processes that would otherwise be difficult to occur in the gas phase[8]. These processes would certainly have a major influence on the chemical budget of atmospheric oxidants.

In spite of extensive research in recent years on the study of atmospheric aerosols, the general knowledge of organic aerosols, their physical properties, chemical composition, sources, transformation and removal processes, is still limited[9]. Consequently, more research is currently ongoing in order to improve prediction, quantitative assessment, and efficient control of atmospheric aerosol effects on global climate and public health[9].

1.2. Objectives

The processing of atmospheric aerosols has been a matter of significant research during the last fifteen to twenty years[10,11]. This research has been carried out in laboratories using model systems (also called proxies) that mimic the characteristics of the real matrix. Subsequent studies[12] have revealed the importance of studying the morphology and structure of the aerosol surface as this is most likely where the reaction mainly takes place. The processes occurring at the surface also define the reactivity, hygroscopicity, and participation of the particle in subsequent processes such as cloud nucleation. To date, probing the surface has proven to be difficult, and it has been especially challenging to eliminate the contribution of any reactive process occurring in the bulk of other proxies used.

Our objective is to develop a system in which atmospheric processing reactions could be studied and followed by recording properties inherent to the surface. The ozonolysis of unsaturated organic compounds is studied, which results in the cleavage of a double bond and therefore, reaction products with shorter alkyl chain length. If the ozonolysis involves the processing of unsaturated compounds forming part of a pure or mixed monolayer at the surface, changes are expected in the characteristics of this surface.

Monolayers can be studied after being transferred to a solid substrate or spread at the air-water interface. For monolayers deposited on solid substrates, the changes of the hydrophobic character of the processed surface can be determined by contact angle measurements. Other surface properties such as surface morphology and monolayer

thickness can be analyzed by atomic force microscopy (AFM) and ellipsometry. The variation in the surface pressure due to reaction can be followed if the monolayer being processed has been spread at the air-water interface of a pendant drop.

The objective of this work is to find a good model system that allows for quantitative determination of the reaction taking place at the surface. By recording changes in the properties of the surface, a kinetic analysis of the processing of atmospheric aerosols could be achieved that has not been previously reported in the literature. Consequently, the possibility and feasibility of an oxidative reaction occurring at an aerosol surface at a faster rate than in gaseous media could be assessed without interference from other ozone uptake processes. The importance of determining this surface contribution has recently been highlighted in the literature[10]. The validity of the system will be examined by comparing the kinetic results obtained to kinetic analysis reported in the literature for the study of the ozonolysis in other model systems. Moreover, a flexible and versatile system would allow setting experimental conditions that mimic the characteristics of an atmospheric aerosol and approximating real life conditions.

Chapter 2

LITERATURE REVIEW

2.1. Atmospheric aerosols

2.1.1. Characteristics and physical properties of atmospheric aerosols

Atmospheric aerosols are defined as mixed suspensions of solid or liquid particles dispersed in a gas medium[3,6]. They can be found in sizes ranging from approximately 0.002 to about 100 μm[6]. Aerosol size distribution and concentration are closely related to the aerosol sources, higher concentrations being found in urban areas rather than over the oceans[3]. The size of the particle also determines its fate and effect on the atmosphere.

Two routes of formation have been described as primary and secondary production of aerosols[1,3]. Atmospheric aerosols can be released into the atmosphere as particulates from natural or industrial dust, sea salt, biological debris, soot, and sand. These are referred as primary aerosol particles. Secondary aerosols are particulates formed by gas-to-particle conversion processes within the atmosphere. An example of this process is the oxidation of SO_2 to sulphuric acid with subsequent association with water molecules, a process that is essential in the formation of acid rain. In general, aerosols are produced by ejection from ocean surfaces, the abrasion by wind action on

biological surfaces (e.g. pollens) or desert sands, combustion processes, either natural or anthropogenic, gas-to-particle conversion processes, and nucleation of smaller particles[3,6].

Atmospheric particles are classified in four main groups according to their size: coarse particles that have a diameter of more than 2.5 μm; particles with diameters between 0.08 and 2.5 μm which are said to form the accumulation range; particles with diameters between 0.01 and 0.08 μm known as the transient or Aitken nuclei range; and finally, those with a diameter smaller than 0.01 μm which are called ultrafine particles[6]. The highest mass distribution is found within the coarse particle range although the highest particle concentration is in the accumulation mode, which also has the largest surface to volume ratio[3].

Coarse particles are usually the result of erosion, wind action, or grinding, and due to their size, they fall out of the atmosphere by sedimentation relatively rapidly. However, coarse particles can be transported over long distances due to convective processes[6]. On the other hand, particles in the accumulation range are formed from the condensation of low-volatility vapors, the result of combustion processes, or by coagulation of smaller particles. Therefore, there is a higher organic content in the accumulation range compared to coarse particles, as well as a higher content of soluble inorganics[6]. As mentioned before, the accumulation range represents a small portion of all aerosols but contain about 50% of the total aerosol mass. They have longer lifetimes that make them very important for atmospheric chemistry studies with considerable effect on cloud formation, visibility and health[6].

Combustion sources like oil-fired boilers or cars produce high-temperature combustion products that enrich the nuclei mode. In addition, atmospheric gas-to-particle conversions produce particles falling in this size range, although these processes can also be the source for the formation of ultrafine particles[6].

2.1.2. Effects of atmospheric aerosols on the climate

Although the contribution of atmospheric aerosols to climate has been difficult to model so far due to their fluctuations in amount, size, and composition[12], it is known that they exert a significant influence in global and regional climate by directly or indirectly affecting atmospheric conditions. An example of a direct effect on climate is seen by how aerosols modify the level of absorption and scattering of incoming solar radiation[1,13], which can decrease the amount of UV-B radiation reaching the earth's surface and induce variations of the planet temperature. Aerosols can act as cloud condensation nuclei (CCN) depending on their size, and chemical composition under high water supersaturation conditions[1]. Thus, these CCN active properties dictate how cloud properties such as reflectance, lifetime, and ability to precipitate are also affected[1]. In addition, they can appreciably have an effect on the chemistry of the atmosphere through heterogeneous and multiphase reactions[6]. Lastly, small size particles can affect human health by penetrating into the respiratory tract and cause inflammation and irritation, and even increase the risk of occurrence of pulmonary and respiratory diseases, among others[3].

2.1.3. Organic composition of atmospheric aerosols

Atmospheric aerosols contain a significant proportion of organic material as determined by field measurement studies[14,15] and confirmed in the laboratory[16-18]. Organic material has been found to be linked to inorganic aerosols, cloud condensation nuclei (CCN), sulphate aerosols, and cloud droplets[1,19]. Marine aerosols, for example, are thought to be comprised of around 10% by mass of organic material[3,8]. The primary sources for the organic constituent of aerosols are diverse as they can be a result of emissions from vegetation, biomass burning, car exhausts, natural gas combustion, cooking exhaust, or the ejection of organic material from the ocean surface[3,10]. In addition, the presence of organic matter in aerosols can be a result of atmospheric condensation of low-volatility organic gases to an aerosol particle[20]. The contribution of these sources depends on atmospheric and meteorological conditions as well as on local characteristics of each region.

In remote non-urban areas different organics can be found such as *n*-alkanes of 15 to 35 carbons, *n*-alkanoic acids and *n*-alkanols of rather an even number of carbons, some monounsaturated fatty acids, and aromatics, among others[6]. In regions affected by anthropogenic emissions, complex organics associated with human activities can be found besides those related to biogenic emissions. As a result, organic compounds such as *n*-alkanes, *n*-alkanoic acids, aromatic aldehydes and acids, polycyclic aromatic hydrocarbons (PAH) and their derivatives, and others, have been found in urban aerosols[6].

Long-chain organic compounds having one or more polar groups, such as carboxylic acids and nitrates, are common in the aerosol composition with either biogenic or anthropogenic origin. For instance, palmitic acid, stearic acid, and oleic acid are fatty acids found in high concentration in aerosols produced from meat cooking[21] or in marine aerosols[17]. These compounds are supposed to act as surfactants in aqueous atmospheric aerosols, likely forming an organic film at the surface of the aerosol[6]. The degree of compression of the surface film would be expected to dictate its effect on water uptake and evaporation in an aerosol particle, the more compressed films being less permeable[6]. Experimental evidence has been found on the increased uptake of water and ammonia by acid droplets coated by hexadecanol when the film is in a condensed state. Likewise, a reduced rate of neutralization of acid aerosol particles by ammonia was observed when the particles were coated with straight chain organic compounds in contrast to when they were coated with branched molecules[6].

Water uptake by a particle conduces to the formation and nucleation of cloud droplets and their growth. The cloud nucleating properties of a particle are described by the Kohler equation[22,23]. According to this equation, cloud droplet growth is favored by a reduction in surface tension, although other factors should be taken into account such as solubility, organic volatility, nature of the particle, and oxidation processes[22]. However, results obtained in experimental systems have shown that changes in surface tension brought about by the presence of organic compounds can increase or decrease water uptake by the particle[24,25]. The effect of the organic coating depends on its composition

and hygroscopic character. Hygroscopic organics were seen to increase CCN properties while water insoluble organic films did not hinder or delay the CCN activation[24].

In general, these changes subsequently dictate how an aerosol participates in cloud formation and cloud albedo[8,20,24]. As a consequence, recent studies focus on the surface activity of organic material in sampled aerosols and cloud water[26]. Additionally, aerosol organic matter reacts with gas-phase species through heterogeneous and multiphase reactions which affect the particle surface properties and alter the atmospheric budget of the corresponding gas-phase species[27,28].

2.1.4. Proposed model of organic atmospheric aerosols

An inverted micelle model has been proposed which describes an organic monolayer covering the air-liquid interface of an aqueous aerosol (Figure 1)[8]. The model consists of an aqueous core that is coated by an inert and hydrophobic monolayer of organic surfactants. Thus, the organic molecules making up the surface film have their polar groups pointing towards the particle core while the aliphatic tails are directed outwards to the atmosphere. This reconciles aerosol organic composition values measured in field experiments with the lack of bulk solubility of organic compounds present in the aerosol[8]. However, Figure 1 depicts an ideal scheme of a real organic aerosol coated by an organic film. Finding a well aligned and ordered monolayer at the air-water interface of this particle would be unlikely because of the diverse and complex composition of the organic aerosol fraction.

The model closely represents sea-salt aerosols which account for the largest source of natural tropospheric aerosols[3]. They are formed by mechanical ejection from the surface of the oceans, acquiring a coating of organic molecules. This organic content has its origin in a thin layer of the remains of cellular decomposition and disintegration, mostly organic surfactants molecules, covering the sea surface. Therefore, the model explains experimental observations by defining the organic coating of the aerosol as mainly composed of large hydrocarbons, with fatty acids as a significant fraction[3]. Inorganic salts and water would be present as well, but water would evaporate as the aerosol rises into the atmosphere, decreasing aerosol size and leaving an organic film coating a brine core[3,8].

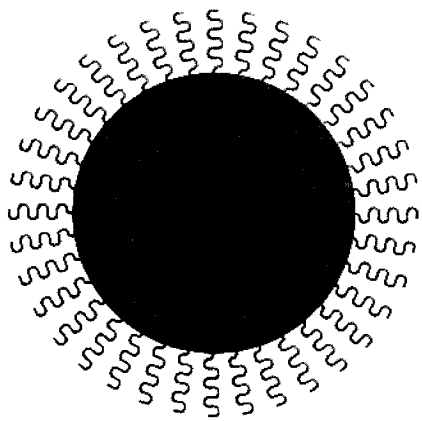

Figure 1: Inverted-micelle model proposed for organic aerosols in which an organic film is coating a core that contains water and inorganic salts.

The proposed model has been confirmed experimentally through several measurements. While the organic composition of aerosols was initially determined to be

high in lipid content[15], evidence of the presence of surface-active carboxylic acids at the surface of collected particles has been found by X-ray spectromicroscopy[29] and electron microscopy[16]. More recent experiments with collected marine aerosols using a scanning electron microscope coupled to an energy dispersive X-ray microanalyzer confirmed the presence of an inorganic core coated by an organic film[18]. These marine aerosol particles were later analyzed by mass spectrometry corroborating the composition, and finding known fatty acids (e.g. palmitic and stearic acids) as main components[17]. On the other hand, a decrease in surface tension in aerosol particles in comparison to cloud droplets has been measured revealing the presence of an organic film[30]. Other soluble organic compounds can also be surface active though, as a higher content of them can be present at the air-water interface compared to their presence in the bulk aqueous phase[12].

The model is applicable not only to explain the organic composition of sea-salt aerosols. Fatty acids have also been found coating the surface of collected sulfate aerosols from continental sources[19]. In addition, fatty acids were found as main components of organic films covering collected ammonium sulfate particles which were studied by atomic force microscopy (AFM) and transmission force microscopy (TFM)[31]. In general, organic and inorganic compounds have been linked to the composition of continental aerosols of both natural and anthropogenic origin[19,32-36].

2.1.5. Processing of organic atmospheric aerosols

Several atmospheric reactions occurring in the condensed phase (at the surface or bulk of liquid or solid particles in contrast to the gas phase) involving atmospheric

oxidants, such as OH radicals, O_3 or NO_3, could take place faster than reactions in the gas phase[3,8,10]. Therefore, reactions occurring at the surface of atmospheric particles would have an appreciable impact on the chemical balance of the atmosphere.

Aerosols with an "inverted micelle" structure would seem to be chemically inert to atmospheric processes and optically inactive[8]. Nevertheless, chemical processing of the organic coating of the aerosol through radical and oxidative reactions could activate it to participate in atmospheric chemistry[8]. For instance, atmospheric hydroxyl radicals can generate a chain of free radical reactions on the aerosol surface with formation of more active species like alcohols, aldehydes, ketones and carboxylic acid groups[8]. Similarly, other oxidants like O_3 and NO_3 will react with this surface whenever double bonds are present[6,8].

2.2. Processing of atmospheric aerosols by ozone

2.2.1. Ozonolysis of unsaturated organic compounds

The ozonolysis of alkenes has been well described in the literature[6,37-40]. The cleavage of a double bond of an unsaturated compound (e.g. an alkene) by an ozone molecule leads to the formation of an unstable primary ozonide (Figure 2). This intermediate species is not stable and decomposes to form a Criegee intermediate and an aldehyde or ketone[6]. The fate of the Criegee intermediate depends on the media in which the reaction takes place. In a condensed phase, a secondary ozonide is formed from the recombination of the Criegee intermediate and the carbonyl compound. This secondary ozonide is stabilized by solvation. In contrast, in the gas phase the decomposition of the

Criegee intermediate leads to the formation of several radical species and small gas molecules.

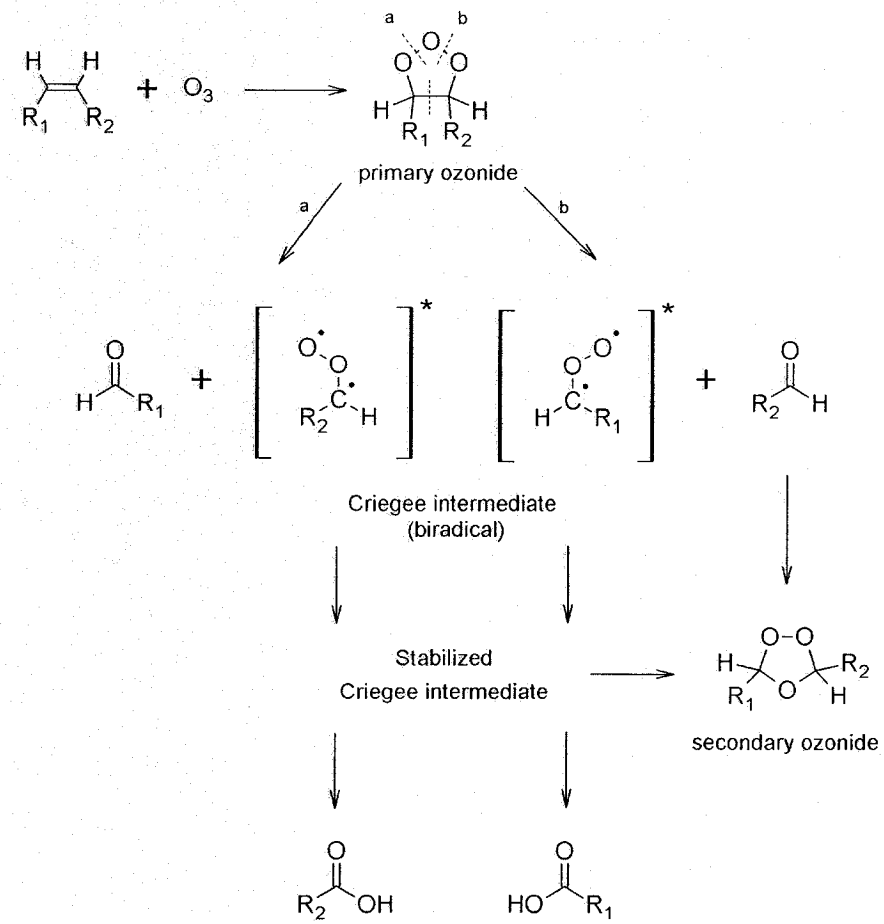

Figure 2: General representation of the processes involved in the ozonolysis of an unsaturated organic compound (based on reference 3).

The reaction of the processing of an unsaturated organic coating by ozone has been studied using different approaches to mimic a real aerosol[10]. The results of these experiments have confirmed the formation of aldehydes and carboxylic acids as the main products of the reaction[39-49].

2.2.2. Consequences to atmospheric processes and chemistry

Hydrophilic sites are created on the surface of the aerosol because of oxidative reactions, which consequently changes its hygroscopic character. The processed surface is thus more hydrophilic and the aerosol can act as a cloud condensation nucleus, which means that it can grow to fog or cloud droplet at suitable supersaturation water vapor conditions[8,20,24]. For example, a recent study of the ozone processing of soot particles, mostly comprised of hydrophobic components, confirmed the creation of polar groups on the surface[50]. On the other hand, the processing of oleic acid droplets has been shown to increase the hygroscopicity of the particles exposed to ozone compared to unreacted particles[51]. As a result, it has been reported that these particles are more hydrophilic and capable to act as CCN[52], although these results were for ozone concentrations higher than real concentrations found in the atmosphere.

It has been suggested that the processing of the aerosol coating film also leaves more chromophores at the surface which can increase light absorption by the particle compared to the aliphatic precursor[8]. Moreover, recent experiments have demonstrated that water condenses more easily on a film of organic acid at a low relative humidity than on a film of alcohols or alkanes[53], thus confirming the effect of the organic film on cloud formation. An increase in particle size has been reported for sea-salt particles coated with oleic acid after being exposed to ozone[46] most likely due to water condensation.

Hence, the oxidation of organic molecules at the surface of an aerosol can increase the effect of the particle on climate by provoking absorption and scattering of incoming solar radiation, and by changing cloud properties like reflectance, ability to

precipitate, rain development and lifetime[2]. Another consequence of this oxidation is the decrease of the atmospheric budget of gas-phase trace species, as well as creating volatile products with the potential to participate in further atmospheric oxidation reactions, which affects the balance of atmospheric oxidants[8].

2.2.3. Kinetics of gas-surface interactions

The reactive uptake of a gas species by aerosols is an example of the heterogeneous reactions that typically occur in the atmosphere where different types of surfaces are available for reaction, from ice crystals to sea-salt particles. The gas-aerosol interaction can be described as the sum of several steps: diffusion of the gas to the surface, accommodation at the surface and transport of the gas across the air-water interface, diffusion of the solvated species into the bulk, and reaction of the species either at the interface or in the bulk of the aqueous phase[6]. The uptake of the gas species by the particle can be modeled using an electric circuit resistance system that includes each of the above mentioned steps either in series or in parallel[6,54]. Each step is represented by an individual resistance Γ, normalized to the rate of gas-surface collisions, and considered to be independent of the others[6,55].

Figure 3 shows a scheme that depicts these processes together with the resistance variables that characterize them. The gas species is initially transported through the gas phase to the surface, which is represented by Γ_g. This process depends on the diffusion of the gas (D_g) and the frequency of gas-surface collisions. Afterwards, the gas species either accommodates at the surface or evaporates back to the gas phase. The efficiency of

this process, including crossing of the interface into the condensed phase, is described by the mass accommodation coefficient α. It is defined as the fraction of gas-condensed phase collisions that lead to the uptake of the gas by the condensed phase[6]. This term is determined by the first order rate constants k_{des} and k_{solv} representing desorption from the surface and entrance to the bulk liquid, respectively, and the probability S representing the probability of adsorption or accommodation at the surface[54].

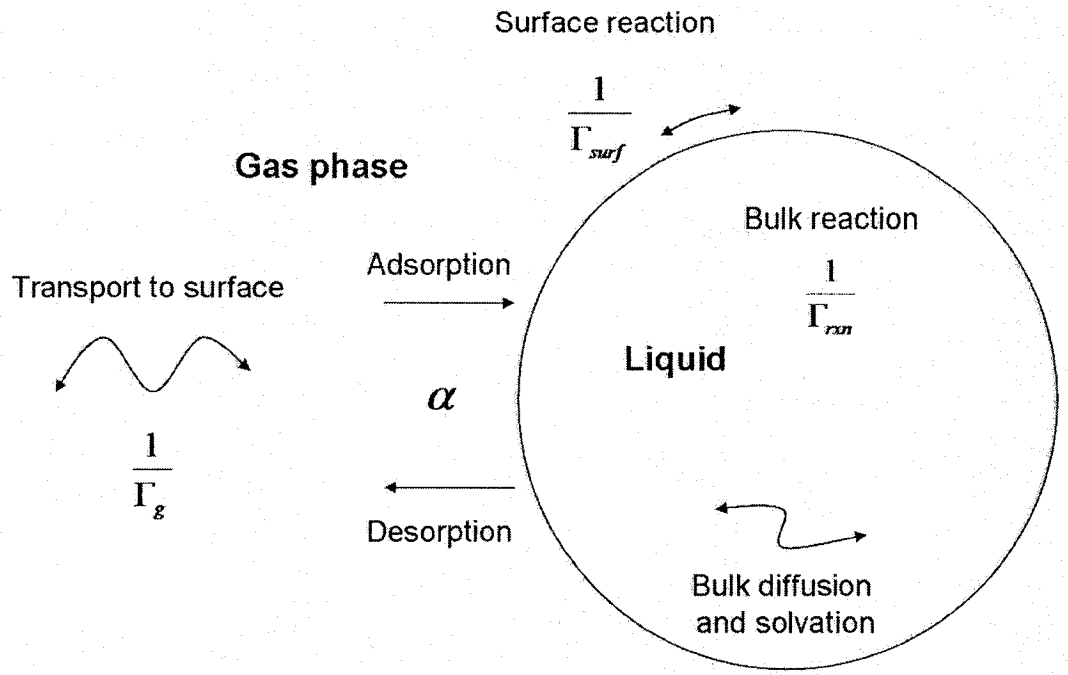

Figure 3: Schematic diagram of the uptake of a gas species by a liquid particle in which each process is represented and described by its corresponding resistance variable (diagram based on a similar scheme described in reference 2).

Next, the gas diffuses to the bulk (D_l), which occurs at a slower rate than the gas diffusion, and is described by Γ_{sol}. The gas-surface system ultimately reaches a dynamic equilibrium, in the absence of reaction, defined by the Henry's law constant H.

Additionally, a reaction could occur either in the bulk (Γ_{rxn}) or at the interface (Γ_{surf}). The reaction is generally treated as being first-order or pseudo-first order, irreversible, and with a rate constant k or k' (where $k'=k[gas]$)[6], assuming the concentration of the gas reactant is high or constant.

The net uptake probability of a gas γ_{net} represents the net rate of uptake, which has been normalized to the rate of all gas-surface collisions. This is the variable commonly measured in reactive or non-reactive uptake experiments and thus, it is denoted as γ_{meas}. A general equation could be described related to this model of gas uptake[6,54]:

(1)
$$\frac{1}{\gamma_{net}} = \frac{1}{\Gamma_g} + \frac{1}{S} + \frac{1}{\Gamma_{surf} + \frac{1}{\frac{S-\alpha}{S\alpha} + \frac{1}{\Gamma_{rxn}}}}$$

The variables on this equation can be calculated from measurable parameters such as the diffusion coefficients D_g and D_l, the Henry's law solubility of the gas H, the mass accommodation coefficient α, and the rate of the reactions in the bulk and at the surface, and therefore, can be used to determine γ_{net}.

By solving this general equation obtained from the application of the uptake model, γ_{meas} is related to the measurable variables (D_g, D_l, H, α) previously described and the variation of the concentration of the gas species due to the reactive uptake[6]. However, the gas uptake has been recently described by focusing on the chemical transformation of the species at the surface of the condensed phase instead of focusing on the concentration of the gas species[54]. The former approach has been used for the development of this thesis research.

2.2.4. Previous studies on the processing of atmospheric aerosol proxies

As atmospheric aerosols are complex systems with diverse composition depending on their source or history, they are difficult to reproduce in the laboratory. Therefore, several model systems, or proxies, have been tested in laboratory experiments[10]. Each proxy typifies a different approach to reproduce one or more characteristics of a real aerosol, which consequently determines the obtained results. Proxies studied include monomolecular organic films[43,56,57], self-assembled monolayers[39-41], frozen and non-frozen organic liquids[10,41,42,44,58-60], liquid droplets[46,51], and laboratory-created aerosol particles[45,47-49,60-63]. The organic compounds utilized in the literature to represent the organic coating of an aerosol are mainly alkenes[39-41,44] and fatty acids[42,47,58,60].

Unsaturated organic liquids were utilized as proxies for flow tube experiments in order to characterize volatile and non-volatile products and thus elucidate chemical mechanisms for the reaction[41,44,47,58,60]. In order to exclude the influence of the bulk on the reaction, these organic liquids have been analyzed as frozen phases as well[42]. The application of chemical ionization mass spectrometry and electron impact mass spectrometry has been essential to accomplish the objectives mentioned above. Product characterization by means of different characterization techniques has established that aldehydes of various chain lengths, formaldehyde, formic acid, and radical species are major volatile products, while carboxylic acids, carbonyls, and dicarboxylic acids are the most probable soluble or surface-bound products of the reaction, depending on the proxy used[10,40,42-44,57,58,60]. In the specific case of the reaction of ozone with oleic acid the major

products of the reaction are 9-oxononanoic, 1-nonanal, nonanoic acid, azelaic acid and high molecular weight compounds[51]. Recent gas chromatography-mass spectrometry (GC-MS) studies have recently corroborated the formation of compounds of high molecular weight in reactions occurring in condensed phase of oleic acid droplets. These products were suggested to be the result of polymerization chain reactions propagated by 9-oxononanoic acid and the Criegee intermediate[51].

A droplet train flow tube apparatus has been used for measuring not only reactive uptake dependence on droplet size but also mass accommodation of the gas, or non-reactive uptake, on the liquid organic droplet[10]. However, a breakthrough in the development of this research has been the use of generated aerosols as proxies together with the use of single particle mass spectrometry[47], which permitted to follow the decrease of oleic acid in an aerosol particle due to the reaction. Experiments with aerosol generators and single particle mass spectrometry found the uptake coefficient to be dependent on the size of the aerosol particle[47] with higher uptake values obtained for small size oleic acid particles. It was suggested that the measured uptake coefficient values were determined by the diffusion of oleic acid within the particle. Also, molecular dynamics computer simulations on monolayers predicted that enhanced kinetics should be observed when compared to that of the gas phase reaction due to trapping of the ozone molecules on the porous organic layer, which then increases the probability of the interaction of ozone with the double bond[43].

Numerous studies have aimed at the determination of the reactive uptake coefficient of ozone. The reactive uptake coefficient is defined as the fraction of

collisions leading to removal of gas-phase species, which means that ozone has been taken up by the condensed phase through reaction. This has been achieved by measuring either the change in concentration of the species at the surface[39,45,47,64] or the rate of ozone lost due to reaction with the proxy[40,41,44,58,59].

The reactive uptake of a gas species by a particle is not only a bulk process but also a surface process. The environment in which the reaction takes place can be determinant to the outcome of the reaction. Recently, aerosol particles have been prepared in the laboratory by coating inert cores of polystyrene latex allowing to probe the reaction with layers of oleic acid ranging from 2 to 30 nm[61]. Relative product yields, reaction rates, and reaction mechanisms were studied as a function of the oleic acid layer thickness. For instance, the percent yields of oxygenated products and 9-oxononanoic acid were seen to decrease and increase, respectively, with increasing layer thickness. Meanwhile, the percent yields of azelaic acid and nonanoic acid were invariable from 2 to 30 nm[61]. This could imply that the mechanism of the reaction goes through different pathways depending on the chemical environmental where the reaction takes place, being at the surface or in the bulk.

Since there is a need for separating surface interactions from bulk contributions, organic film monolayers have been utilized as proxies. Self-assembled monolayers on glass substrates have been primarily studied as they represent well-ordered systems where surface functional groups can easily be controlled and identified[40,41,43]. Infrared spectroscopy has probed the outcome of the reaction on thin films by providing quantification of gas-phase products above the location of the reaction as well as

condensed-phase products[40,60]. In this case, the reaction was monitored by following the variation in the concentration of either ozone, the organic compounds in the liquid or surface, or their products. A recent report described real-time monitoring of the oxidative reaction of a self-assembled monolayer of vinyl compound by ATR-FTIR[39]. Infrared spectroscopy has also been applied to the study of the reaction at the air/water interface. Voss *et al.* utilized both surface-specific, broad-bandwidth, sum frequency generation spectroscopy (BBSFG) and infrared reflection absorption spectroscopy (IRRAS) to follow the ozonolysis of an oleic acid monolayer[65]. Since BBSFG utilized the alkyl stretching bands to follow the disappearance of the reactant from the surface, no specific chromophore is required, although deuterated reactants were required to study mixed monolayers[66]. This real-time monitoring of the reaction requires highly specialized techniques and instrumentation.

Some studies have focused specifically on reactions occurring at the aerosol surface. In an early report, Srisankar *et al.*[56] exposed compressed monolayers of oleic acid and linoleic acid to low concentration ozone aliquots. They confirmed the effects on the physical properties of the monolayers, detecting a decrease in measured surface pressure[56]. They also observed a first order behavior in the contraction of the monolayer at constant surface pressure. This kinetic behavior has been later confirmed by other methods[41,42,44,58], suggesting that the reaction rate is independent of the ozone concentration. Recent experimental results found that the reaction follows a Langmuir-Hinshelwood mechanism in which the rate-limiting step in the uptake of ozone is the accommodation at the surface with reaction occurring afterwards. This behavior has been

reported for the reaction of ozone with vinyl-terminated self assembled monolayers[39], anthracene and other PAHs adsorbed at the air-water interface[64,67,68], and benzo[α]-pyrene on soot particles[69].

Other relevant experiments include those of Wadia *et al.*[43] and Mmereki *et al.*[64], who studied the reaction of ozone with organic compounds located at the air-water interface. Wadia *et al.* exposed unsaturated phospholipid monolayers to ozone and followed the reaction by measuring the gas-phase products using mass spectrometry. Mmereki *et al.* applied a more direct approach for monitoring the surface reaction by measuring changes in the fluorescence of anthracene adsorbed at the air-liquid interface. Applying this technique has also permitted recently a kinetic study of the ozonolysis of other PAHs, such as naphthalene, fluoranthene, phenanthrene, pyrene, and benzo[a]pyrene, at the air-water interface[67]. However, this type of experiment requires the presence of a chromophore in the molecule in order to monitor the reaction spectroscopically. A broad range of organic compounds do not fulfill this requirement, in particular phospholipids and fatty acids, which have been identified as major aerosol components[6,15]. Also, it is worthwhile to mention the work by Dubowski *et al.*[39] who studied the real-time oxidation by ozone of self-assembled monolayers (SAMs) of terminal alkenes on a silicon crystal using in-situ attenuated total reflection infrared spectroscopy (ATR-FTIR). This technique offers some improvement as no specific chromophores are required, but SAMs on solid substrates may not be an ideal proxy for liquid aerosols.

Most recently, research has focused on the study of model systems in which humidity is also controlled and its effect on the reaction rates and products also assessed[61]. Attempts have also been made to characterize the reaction in mixed systems of unsaturated and saturated compounds, for example, by studying the ozonolysis of generated aerosol particles of mixed oleic acid–stearic acids compositions[62]. Likewise, mixtures of oleic acid with myristic acid and lauric acid, both saturated, were studied in a rotating-wall flow-tube reactor looking at how the mixture phase and structure affect the kinetics of the reaction[59]. The authors emphasized in their conclusions the need for a separation between the contributions of the surface and the bulk reactions.

Current research has revealed the importance of studying the surface activity of atmospheric aerosols. For example, measurements of surface tension on collected aerosol samples found a strong relationship between surface activity and the concentration of water-soluble organic compounds[26]. As mentioned before, in the case of oleic acid (a fatty acid containing an eighteen carbon chain which is commonly used for proxy studies[42,45-49]), when reacting with ozone, the double bond is cleaved forming either nonanal or nonanoic acid, azelaic acid, octanoic acid, and 1,9-nonadioic acid or 9-oxononanoic[10,42,46,51]. Therefore, the exposure of a surface layer of oleic acid to ozone results in the formation of products more hydrophilic than oleic acid and with much shorter chain lengths. High molecular weight products have also been detected which could possibly increase the viscosity and hydrophobicity of the surface after the reaction[51]. However, no evidence has been found of any oxidized products remaining at

the surface after reaction[65], since they either evaporate, as in the case of nonanal, or dissolve into the subphase.

Consequently, the products of the reaction have less surface activity than oleic acid due to their higher solubility in water. This change in surface activity reflects changes in composition at the surface and therefore, the reaction can be followed by measuring how the surface tension (related to surface coverage) varies with the progress of the reaction. The approach of this research was to develop a suitable model system and necessary experimental conditions for following the reaction, assuming that it takes place mainly at the surface as has been proposed by several studies and computer simulations. For this purpose, the surface in question has to be characterized before and after reaction through a surface property that quantitatively changes because of the reaction.

Chapter 3

MATERIALS AND METHODS

3.1. Chemicals

Phospholipids (Table 1) such as 1,2-dioleoyl-*sn*-glycero-3-phosphocholine (DOPC), 1,2-dipalmitoyl-sn-glycero-3-phosphocholine (DPPC), 1,2-dimyristoyl-*sn*-glycero-3-phosphocholine (DMPC), and 1,2-distearoyl-*sn*-glycero-3-phosphocholine (DSPC) were purchased from Avanti Polar Lipids, all having a purity of 99% or more. Fatty acids (Table 2), such as oleic acid, stearic acid, brassidic acid, elaidic acid, erucic acid, and linoleic acid were purchased from Sigma-Aldrich with similar purity.

Chloroform (HPLC grade) was used for the preparation of most of the solutions, and it was acquired from Fisher. Fresh ultrapure water (18.2 MΩ·cm) obtained from an Easypure II LF system (Barnstead) was used for trough and drop experiments. Hydrochloric acid (Merck), sulfuric acid (J. T. Baker), and methanol (Fisher, purity of more than 99.8%), were also used.

Table 1: Summary of phospholipids used in this project.

Structure		
Abbreviation	Molecular Formula	Name
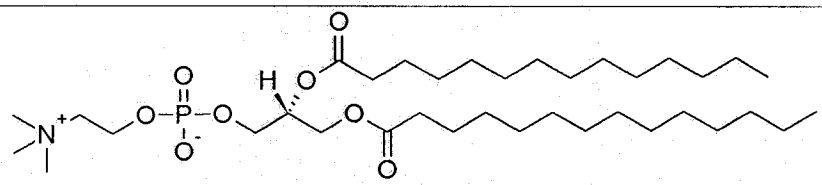		
DMPC	$C_{36}H_{72}NO_8P$	1,2-dimyristoyl-*sn*-glycero-3-phosphocholine
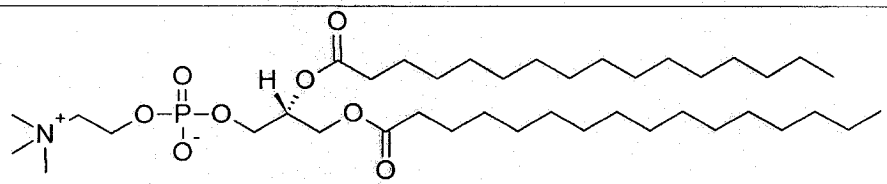		
DPPC	$C_{40}H_{80}NO_8P$	1,2-dipalmitoyl-*sn*-glycero-3-phosphocholine
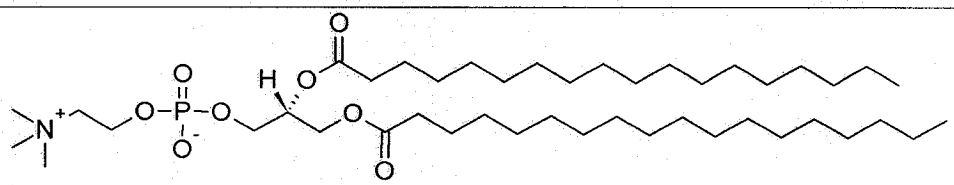		
DSPC	$C_{44}H_{88}NO_8P$	1,2-distearoyl-*sn*-glycero-3-phosphocholine
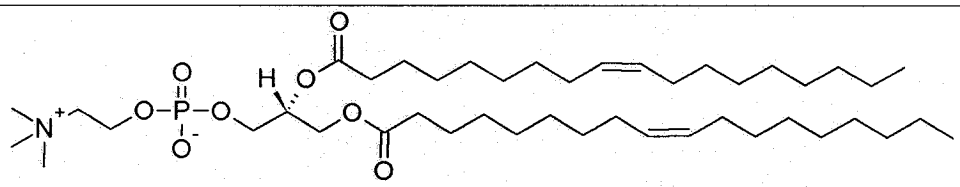		
DOPC	$C_{44}H_{84}NO_8P$	1,2-dioleoyl-*sn*-glycero-3-phosphocholine

3.2. Experimental techniques on a Langmuir film balance

3.2.1. Compression of a monolayer spread on a film balance

The basis of the film balance technique for the analysis of the properties of an air-water interface film has not changed much since initially developed by Pockels[70] and Langmuir[71]. A trough filled with water has one or two Teflon barriers that run over the water surface, increasing or decreasing the area enclosed within. A piece of filter paper or a wire immersed in the water can act as a Wilhemy plate[72], and used to measure surface tension as the plate is pulled down by the effect of the surface tension. The surface pressure π exerted by the monolayer is defined as the difference of the surface tension of pure water γ_0 compared to the surface tension γ measured when a monolayer is present on the surface.

A solution of a surfactant with low water solubility is spread on the surface area within the barriers. As a result, a monomolecular thin film is formed, and compression is achieved by decreasing the area where the monolayer is enclosed. Figure 4 shows a schematic representation of a surface pressure versus molecular area isotherm as the monolayer undergoes structural changes at the surface. Depending on the level and type of interactions among the molecules composing the monolayer, different two dimensional phases can be seen during compression. These phases are analogous to those experienced when performing a three dimensional compression of a gas, and their presence has been confirmed by optical, microscopic, and diffraction techniques[73].

Table 2: Summary of all analyzed fatty acids.

Common name	Molecular Formula	Chemical structure
Stearic acid	$C_{18}H_{36}O_2$	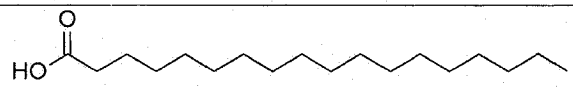
Arachidic acid	$C_{20}H_{40}O_2$	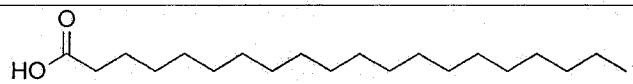
Oleic acid	$C_{18}H_{34}O_2$	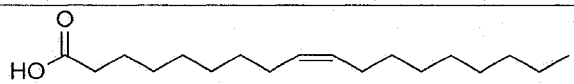
Elaidic acid	$C_{18}H_{34}O_2$	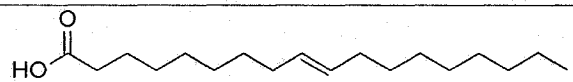
Linoleic acid	$C_{18}H_{32}O_2$	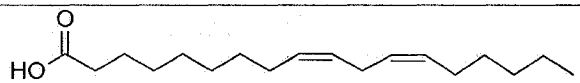
Erucic acid	$C_{22}H_{42}O_2$	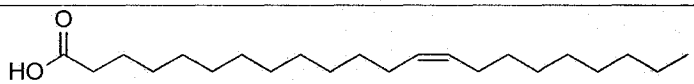
Brassidic acid	$C_{22}H_{42}O_2$	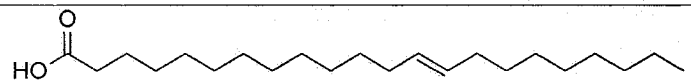

In Figure 4, three general states are shown: a gaseous phase at low surface pressure values, followed by a liquid expanded phase, and finally, condensed phases of either tilted or untilted molecules. As in the gas compression analogy, phase transitions are observed from one phase to the other, represented in the isotherm either by a plateau of phase coexistence or by a kink of the surface pressure curve. The transition from a liquid expanded phase to a condensed phase, observed as a plateau, is a first-order transition that occurs at higher surface pressures with increasing subphase temperatures.

The kink observed with further compression corresponds to a second-order transition in which there is a substantial change in compressibility of the monolayer. The difference between the phases involved in this transition is based on the orientation of the chains with respect to the water surface, going from tilted to perpendicular.

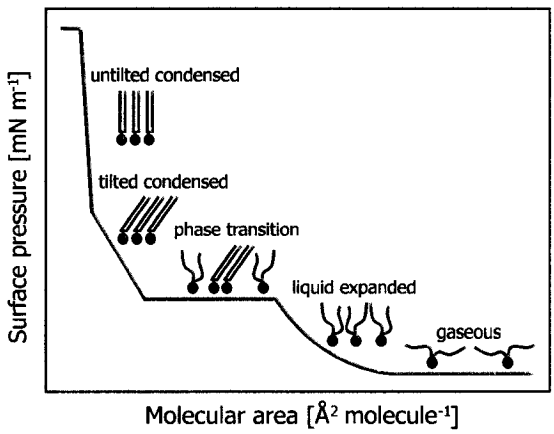

Figure 4: Schematic representation of the compression of a monolayer spread at the air-water interface, where general states of the monolayer have been indicated on the curve.

Lastly, the compression isotherm obtained is characteristic of each monolayer, which is directly related to the chemical structure of the molecules at the surface. However, it also depends in other experimental conditions such as temperature, and composition and pH of the subphase.

3.2.2. Preparation and spreading of a solution

A sufficient mass of the lipid was weighed to obtain a chloroform solution of a concentration of about 1 mM in a volumetric flask (Pyrex). The spreading of the solution

on a Langmuir trough (Nima Technology Ltd) was carried out by taking a known volume of the prepared solution, between 5 to 20 μL, with a Hamilton syringe. The solution was released in short steps by touching the surface with a drop of solution formed at the tip of the microsyringe within the area enclosed by the trough Teflon barriers. Thus, a monolayer of the lipid was formed at the air/liquid interface. After depositing the monolayer, the chloroform was allowed to evaporate for at least 2 min, before starting any compression.

3.2.3. Compression of a monolayer

A compression isotherm of a monolayer was obtained by decreasing the surface area enclosed within the trough barriers. The usual barrier speed for compression was 5 $cm^2\ min^{-1}$ (which corresponds to 0.09 $Å^2\ molecule^{-1}\ s^{-1}$, for a spread volume of 12 μL of a typical oleic acid solution). The compression of a monolayer was carried out up to the monolayer collapse. A compression isotherm is represented as a plot of surface pressure versus molecular area. The molecular area was determined as the ratio of the number of molecules spread at the surface and the surface area.

3.2.4. Langmuir-Blodgett transfers

The Langmuir-Blodgett technique is widely used for the deposition or transfer of a monolayer onto solid substrates such as silicon, mica, and glass. All monolayers were transferred to either silicon wafers (Wafer World, one-side polished, type N, with phosphorus as dopant, orientation 100, and resistivity of 1-20 Ω·cm) or highest V1 grade muscovite mica sheets (Ted Pella). Silicon wafers were cleaned before use by exposing

them first to a $HCl:CH_3OH$ (1:1) mixture for 30 min, then they were rinsed with water, and later exposed to concentrated H_2SO_4 for other 30 min. Afterwards, they were washed with ultrapure water and dried using a stream of clean air. Mica was previously cleaved by separating a fine layer from each side of the wafer, which leaves a fresh surface for depositing a monolayer.

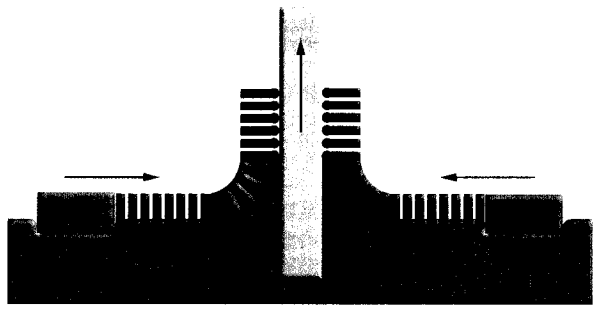

Figure 5: Schematic representation of the transfer of a monolayer onto a solid substrate (e.g. mica): the solid substrate is removed from the water while the compression applied by the trough barriers ensures the surface pressure is held constant.

The monolayer transfer was performed by immersing the solid substrate perpendicularly into the water before spreading any solution. Spreading and formation of the monolayer were performed as explained before. The monolayer was compressed to the desired surface pressure, and afterwards, the film was transferred to the solid as the solid substrate was moved vertically upward from the water, commonly at a speed of 2 mm min^{-1} (Figure 5). The surface pressure was held constant during the transfer by controlling the area within the barriers.

The quality of the transfer was determined by calculating the transfer ratio, which is equal to the monolayer area transferred (obtained from the graph of surface area versus time), divided by the area of the solid substrate on which the monolayer was transferred. The transfer of a monolayer to a solid substrate is considered good when its transfer ratio value falls between 0.8 and 1.2.

3.3. Contact angle measurements

In order to determine the contact angle of water on a monolayer deposited on a solid substrate, a drop of water was placed on the surface and an image of the resulting sessile drop was captured by the camera of the PAT-1 surface tensiometer (Sinterface Technologies).

Figure 6: Determination of the contact angle of a water drop over a monolayer of DMPC:DOPC (2:1) showing the observed loss of hydrophobicity due to reaction, *Left*: Schematic representation of the measurement, *Center*: after transfer of the monolayer, *Right*: after exposure to ozone.

The contact angle was determined by measuring the angle formed by the drop-substrate contact baseline and a tangent to the drop profile at the baseline (Figure 6). Ten measurements were taken on each side of the drop and averaged.

3.3.1. Ozone exposure of a monolayer deposited on a solid substrate

After transfer of a monolayer and measurement of the contact angle, the samples were allowed to dry overnight before being exposed to ozone in an UVO-Cleaner (Jelight Company) at a concentration higher than 30 ppm. The ozone concentration was determined by means of an ozone monitor (2B Technologies). The contact angle was then measured for each sample after exposure to ozone and the variation in contact angle was calculated as the difference of the two measurements, before and after exposure. At least three samples were analyzed for each exposure time. Each sample was transferred independently and exposed to ozone only if a reasonable transfer ratio value was obtained for the previous monolayer transfer. The average change in contact angle was calculated for all samples at each time of exposure.

A sample that was not exposed to ozone was used as a standard and analyzed together with the rest of the samples. It was identified as a zero minute exposure sample. Any variation of the contact angle observed for this unexposed sample was found to be within the measurement error, and the result of monolayer exposure to the environment.

3.4. Atomic force microscopy

Atomic force microscopy (AFM) is a very efficient technique for imaging almost any flat solid surface at ambient conditions and with resolution down to the atomic

level[74]. The instrument consists of a sharp tip, attached to a cantilever, scanning over the sample. The cantilever works as a force sensor that senses any forces of repulsion or attraction between tip and sample. The deflection of the cantilever due to the interactions with the sample is measured by the deviation of a laser beam that bounces off the cantilever and is optically detected afterward. The tip-sample interactions are thus observed as the topography of the sample.

Two main working modes are commonly used in AFM for measuring the topography of the surface. In contact mode, the tip is constantly touching the surface and the cantilever deflection is recorded while the surface is scanned[75]. In some cases, this mode could be inconvenient when working with soft and easily modifiable samples. In tapping mode, the cantilever is excited to oscillate close to its resonance frequency, and therefore, the tip does not contact the surface in a continuous manner. Due to interactions with the sample surface there is a phase shift of the cantilever oscillation relative to the periodically applied signal that drives the cantilever, which is simultaneously recorded. Through this approach, the effect of lateral forces between tip and sample are reduced, therefore, soft samples are easier to analyze[75]. In addition, the contrast seen on phase imaging contains a topography contribution together with information on sample properties such as viscosity, adhesion, wetting, and surface charges, a result of surface composition[76-78]. Therefore, although images showing height differences at the surface were the main scope of the analysis, phase contrast images were also used when they proved to be useful for obtaining more information about the analyzed sample.

The surface morphology of the samples transferred to either mica or silicon was analyzed by means of a Nanoscope IIIa (Digital Instruments). Images were captured in air at room temperature using tapping mode (medium damping, ~ 25%), an oscillation amplitude of 175 mV, and mainly at a scan rate of 2 Hz. Lower scan rates were applied when scanning a larger size of the sample (20 μm and higher). Etched silicon cantilevers (RTESP Nanoprobe, Veeco) used had a nominal spring constant of 20-80 N m^{-1}, resonance frequency values around 300 kHz, and a tip radius of < 10 nm.

Analysis was carried out for two or three independently transferred samples for each pure lipid or lipid binary mixture. Likewise, at least three different areas were scanned for each sample. In some cases, the scan angle of a sample was changed (usually 90°) looking for any dependence of surface features to the transfer direction.

3.5. Ellipsometry

Ellipsometry is an optical technique based on the detection of the changes in polarization encountered on a beam of light reflected from a surface in comparison to the polarization of the incident beam[79]. In a common experiment, the incident beam is polarized elliptically by passing through a polarizer and a compensator. After the reflection from the sample surface, the light becomes linearly polarized, which is examined by means of an analyzer. This technique permits the characterization of a surface regarding the film thickness of either single monolayers or multilayer, as well as the refractive indices of all layers present at the surface.

3.6. Experiments on a pendant drop

A PAT-1 Drop and Bubble Profile Analysis Tensiometer (Sinterface Technologies) was utilized which uses axisymmetric drop shape analysis (ADSA) to monitor changes in surface tension, volume, and surface area of a pendant drop created at the end of a stainless steel capillary. The volume of the drop can be either increased or decreased by releasing water to the drop or withdrawing water from it, respectively. The water volume is controlled by means of a motorized microsyringe, which is connected to the capillary by a thin tube. The pendant drop is placed inside a chamber in which it is protected from contamination and air currents. or a sessile drop on a solid surface

3.6.1. Axisymmetric drop shape analysis

An alternative to the Wilhemy plate technique for the measurement of surface tension is found through axisymmetric drop shape analysis (ADSA), which is a method based on the fitting of the shape profile of a drop to theoretical drop shape profiles obtained for known surface tension values[80-82]. The technique can be applied as well to measurements of contact angles at liquid-solid surfaces.

A pendant drop is subjected to the combined effect of both surface tension and gravitational forces, which determine its shape. The Laplace equation for capillarity links the pressure across a curved interface to the surface tension and curvature of the interface:

(2) $$\gamma\left(\frac{1}{R_1}+\frac{1}{R_2}\right)=\Delta P$$

In equation 2 γ is the surface tension, R_1 and R_2 represent the radii of curvature, and ΔP is the pressure difference across the interface. If no other external force than gravity is acting on the interface, ΔP can be expressed as a function of the height with respect to a reference plane:

$$\Delta P = \Delta P_0 + (\Delta\rho)gz \tag{3}$$

where ΔP_0 is the pressure difference at the reference plane, $\Delta\rho$ is the density difference between the two bulk phases, g is the gravitational force, and z is the height from the reference plane to any point of the curvature where ΔP is calculated. Therefore, using these two equations the shape of the drop is determined for each value of surface tension. Real measurements, acquired by taking images of the drop, are fitted to calculated theoretical drop shapes. An accuracy of ± 0.1 mN m^{-1} is obtained for the calculation of the surface tension due to the application of this method.

3.6.2. Monolayer compression on a pendant drop

A solution of oleic acid or phospholipid in chloroform of a concentration 0.1 mM was prepared by dilution of a 1 mM solution prepared before. For the spreading of a lipid monolayer, a known volume of this solution, from 0.4 to 0.9 µL, was taken with a microsyringe. The monolayer was formed at the surface as the chloroform solution was released in short steps while slightly touching the drop surface with the tip of the syringe (Figure 7). This procedure was monitored using a camera with the purpose of avoiding the penetration of the syringe needle into the bulk of the drop. The volume of the drop when spreading was smaller than the initial drop volume for the experiments to avoid the

drop detaching from the capillary since the surface tension decreases considerably with spreading of the solution. After spreading, the drop was left for 2 min for evaporation of the chloroform before being placed in the reaction chamber (of approximate volume of 28 cm^3). The size of the drop was then increased to ensure that compression began at a point in the isotherm at which the molecular area was high enough for the monolayer to be found in a gas-analogous state. Finally, a further 3 min standing time was allowed for stabilization of the drop as well as to ensure complete solvent evaporation.

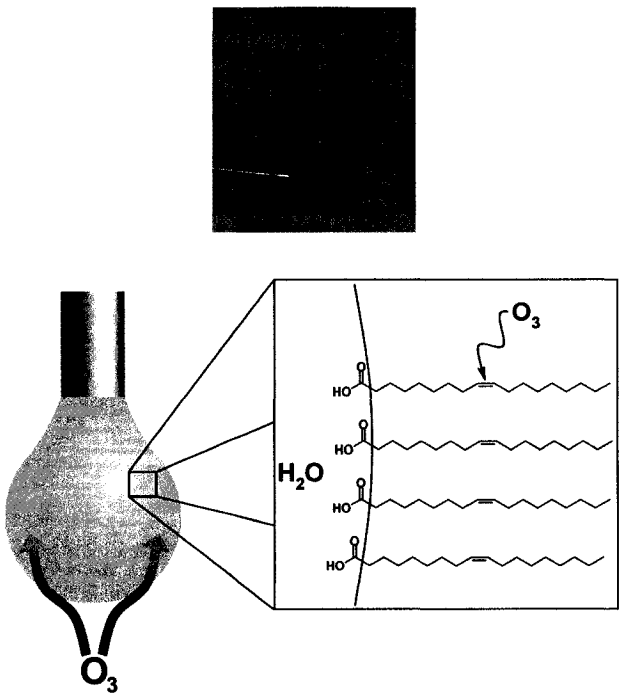

Figure 7: Schematic representation of the model system used for the processing by ozone of a monolayer of oleic acid spread on the surface of a pendant drop. The top figure shows how the monolayer was spread on the drop.

A compression isotherm of the deposited monolayer was obtained by decreasing the surface area. The drop surface area decreased when water was withdrawn in a controlled manner from the drop. Each monolayer compression started at a drop surface area of 0.4 cm^2. After 1 min at constant area, the drop surface area was slowly decreased at a rate of 6×10^{-4} cm^2 s^{-1} (which corresponds to a decrease of 0.13 $Å^2$ $molecule^{-1}$ s^{-1}, for a spread volume of 0.6 μL of an oleic acid solution) as determined using ADSA. The compression was stopped at surface areas of 0.1 to 0.15 cm^2, at which point the compression isotherm indicated that the monolayer had already reached its collapse pressure. A compression isotherm was represented as a plot of surface pressure versus molecular area, as explained above for the compression of a monolayer on a film balance. Although the change in surface area was determined indirectly from the change in volume, at the drop volumes used in all drop experiments the relationship between them was linear[80].

3.6.3. Ozone exposure of a monolayer deposited on a pendant drop

An experimental set up was developed for the exposure of monolayers to ozone and real-time monitoring of the reaction as shown in Figure 8, which we previously reported[83]. Air is passed through a Drierite gas drying unit containing anhydrous calcium sulfate in order to eliminate water. A VOC scrubber and a ChromGas zero air generator (Parker) were placed downstream to produce hydrocarbon-free air. Ozone was generated using a Pen-Ray lamp (UVP, wavelength 185 nm, power 2 to 20 watts) and the ozone concentration was measured directly before entering the reaction chamber by means of an

ozone monitor (2B Technologies) according to the level of absorption of UV light at 254 nm. The range of ozone concentrations to which monolayers were exposed represents typical atmospheric ozone values as well as concentrations found during pollution episodes.

The same procedure described for carrying out the compression isotherms was followed for the exposure experiments. For instance, Figure 9 shows a graph plotted with the obtained data during the exposure experiment, which was monitored by measuring surface pressure and ozone concentration, and following the progress of the reaction. However, detailed data analysis is presented in the next section of this thesis.

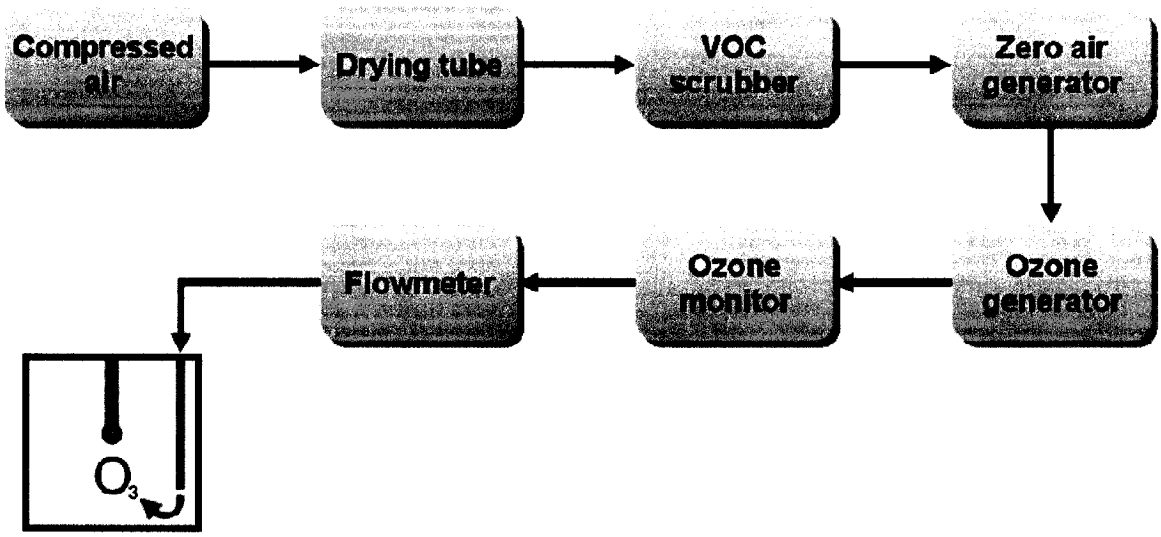

Figure 8: Scheme showing the experimental set up used for carrying out the exposure to ozone of a monolayer spread on a pendant drop.

For this example experiment, 0.6 μL of an oleic acid solution were spread on the drop surface. After evaporation of the solvent and drop equilibration, the compression

was started and simultaneously, air with no ozone was allowed to flow into the chamber. The compression was stopped at 0.2 cm^2 (around 0.01 cm^3 in drop volume) and the drop was held at this surface area; this corresponds to a surface pressure of about 20 mN m^{-1}. When the surface pressure reached a stable value (about 25 minutes after stopping compression of the monolayer), ozone was allowed to flow into the reaction chamber at a rate of 100 cm^3 min^{-1} and a concentration of about 8 ppm in air.

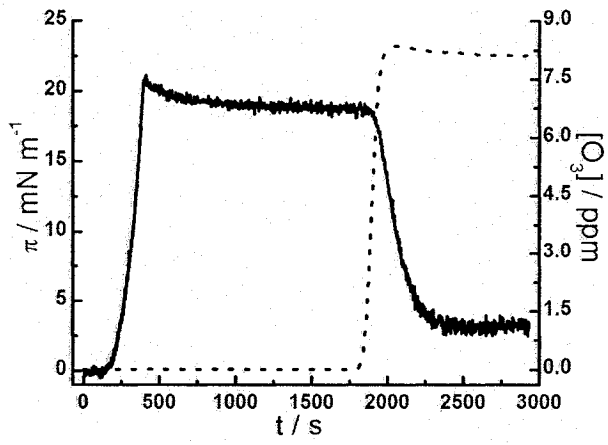

Figure 9: Exposure to ozone of a monolayer spread on the surface of an aqueous drop (initial surface area 0.4 cm^2): surface pressure π (solid lines), ozone concentration (dashed line). The mixture of ozone and air was flowed at 100 cm^3 min^{-1}. (The monolayer was deposited using 0.6 μL of a 0.1 mM spreading solution of oleic acid in $CHCl_3$)

The surface tension at the drop surface is known on a real-time basis (images are acquired at a rate of up to 25 images per second). This method also generates values of the volume and the surface area of the drop, either of which can be controlled by releasing or withdrawing water to and from the drop through an automated motorized

microsyringe. Controlling the drop surface area allows measurement of monolayer isotherms as well as variation of drop size for monitoring the reactive exposure of the monolayer to ozone.

In general, the average starting surface pressure for all exposure experiments, right before beginning of the reaction, was 20 mN m^{-1}. Given the frequency at which drop images were captured, the section of the curve representing the reaction with a decrease in surface pressure contained from 60 to more than 1000 points depending on how fast the reaction took place (which was directly related to ozone concentration). Exposure experiments of other monolayers of different composition were carried out in the same manner. Initial solution volumes spread on the drop surface depended on the surface pressure at which the reaction was aimed to occur, and ozone concentration was regulated as desired. All experiments were carried out at room temperature (296 K).

Chapter 4

RESULTS AND DISCUSSION

4.1. Introduction

As described in the second chapter, the objective of this project was to find means for monitoring the progress of the processing by ozone of unsaturated organic monolayers by looking at changes in the properties or characteristics of a surface film. The reaction of ozone with unsaturated organic compounds occurring at a surface, either solid or liquid, would involve the cleavage of the double bond and formation of several possible products. This would undoubtedly lead to modifications of the surface, likely to be observed as changes in surface topography, morphology, height, surface activity or hydrophobicity. The overall goal of the project also was to obtain results by mimicking as close as possible the structure of the inverted micelle model for organic aerosols.

Therefore, an initial step would be to search for the most efficient system to meet those said requirements. Each system would have to be analyzed before and after exposure to ozone looking for a measurable evidence of the reaction. An effective system would lead to a more insightful study of the process: a more robust kinetic analysis, an examination of its versatility, and the comparison to reported results in the literature.

4.2. Characterization of fatty acid monolayers

The aim of this research was to develop a system for the characterization and monitoring of the processing of monolayers by ozone. The studied monolayers contained unsaturated organic compounds as the only component or as part of a binary mixture. Any measurable surface property of a monolayer would be directly related to the behavior of the selected surfactants or mixture of surfactants at the air-liquid interface. For this reason, several compounds were characterized when spread at the water surface of a Langmuir film balance.

A selection of unsaturated fatty acids was studied with different alkyl chain lengths, and different number and position of the unsaturations. In addition, saturated fatty acids such as stearic acid and arachidic acid were characterized for comparison. They were used in control experiments and for preparing binary mixtures. Table 2 in the previous section presents the name, molecular formula, and structure of all characterized fatty acids, which were chosen since they have been determined to be significant components of collected atmospheric aerosols[6].

All compounds in Table 2 form insoluble monolayers due to the amphiphilic character of their molecular structure. Figure 10 shows the isotherms obtained for the studied fatty acids. The influence of the molecular structure on the compression isotherm could be observed in Figure 10, *Left*, for fatty acids containing 18 carbons. Stearic acid can be compressed up to a small critical area value. At this point the surface pressure rapidly increases because of the formation of a condensed phase, in which all saturated molecules form a densely packed film. A second order phase transition is observed as a

kink at about 25 mN m^{-1}, when the orientation of the molecules in the monolayer changes, forming an untilted condensed phase[73]. A similar behavior is observed for arachidic acid, the other saturated fatty acid analyzed.

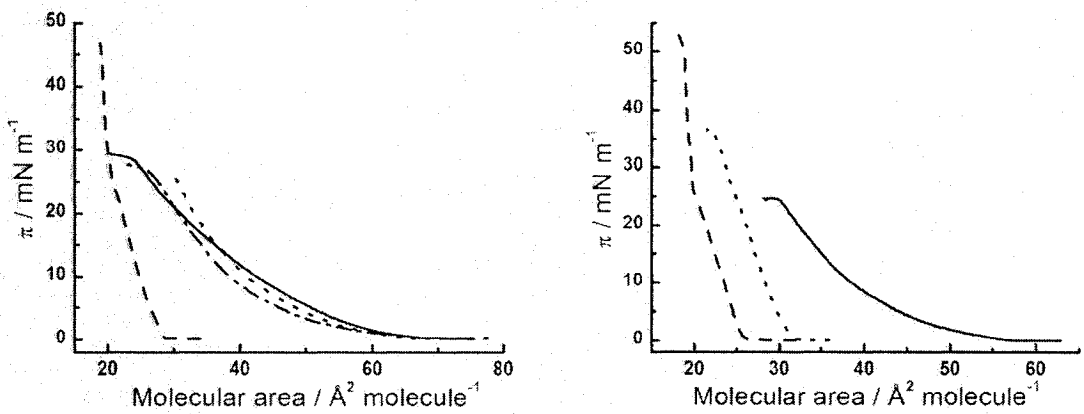

Figure 10: Compression isotherms of studied fatty acids on a Langmuir film balance. *Left*: stearic acid (dashed line), oleic acid (solid line), elaidic acid (dotted line), and linoleic acid (dashes and dots). *Right*: arachidic acid (dashed line), erucic acid (solid line), and brassidic acid (dotted line).

Unsaturated fatty acids having a *cis* conformation in the double bond tend to remain in a liquid expanded phase throughout the compression as their bent structure hinders getting a closer packing of the monolayer[84]. This behavior was observed for oleic acid, linoleic acid, and erucic acid. On the other hand, *trans* isomers have straighter chains which facilitate closer lateral interactions among molecules, leading to the formation of condensed phases[84], as could be seen for brassidic acid. However, elaidic acid did not show this behavior, as it has been reported that a transition to condensed

phase for a monolayer of this fatty acid is only observed at temperatures below 20°C[85]. In general, the isotherms obtained are in agreement with those reported in the literature for these compounds[86-88].

4.3. Ozone exposure of a monolayer deposited on a solid substrate

4.3.1. Preliminary study of contact angle measurements

Initially, several monolayers were prepared and transferred to solid substrates and later exposed to ozone. The cleavage of the unsaturation by ozone produces reaction products with shorter chain lengths, mainly with carboxylic acid or aldehyde functional groups[38]. Previous studies have distinguished nonanal as the only volatile compound among the main products of the reaction. Other products remain at the surface, which consequently decreases the hydrophobic character of the surface. Therefore, the objective was to verify the possibility of using the measurement of the contact angle of water with these surfaces as a variable for monitoring the changes in hydrophobicity and characterizing any other possible effect on the surface.

Table 3 shows the results of a preliminary study that was carried out in order to find the best experimental conditions for measuring the contact angle of a monolayer before and after exposure. Appreciable contact angle changes due to exposure should be observed to provide useful data about the reaction. In the table, θ_I and θ_F represent the contact angle values before and after exposure, respectively, while $\Delta\theta$ represent the variation or difference between the two measurements. One sample was analyzed for

each case, and the error values represent 2σ of the visual measurements applied to each individual sample.

Table 3: Preliminary results of the exposure to ozone of different monolayers on either silicon or mica for 5 min ($[O_3] > 30$ ppm).

		θ_I (°)	θ_F (°)	$\Delta\theta$ (°)
Oleic acid	Silicon	22 ± 2	N/M	>10
	Mica	51 ± 2	N/M	>40
Stearic acid : Oleic acid (1:1)	Silicon	22 ± 1	N/M	>10
	Mica	57 ± 1	41 ± 2	16
DSPC : DOPC (2:1)	Silicon	43 ± 1	36 ± 2	7
	Mica	90 ± 1	80 ± 2	10
DMPC : DOPC (2:1)	Silicon	37 ± 1	32 ± 2	5
	Mica	84 ± 1	72 ± 2	12

N/M: Not measurable

It can be seen that monolayers of oleic acid, pure and mixed with stearic acid, yielded low values for the contact angle after being transferred, evidence that the monolayer is not closely packed. Monolayers of pure oleic acid completely reacted which explains the appreciable loss of hydrophobic character of the surface after 5 min of ozone exposure. This result can be related to reports by Asad et al[89] of a rapid increase of water uptake by oleic acid films after ozone exposure as a result of the surface being more

hydrophilic. The recorded water uptake depends on the ambient relative humidity and time of exposure[89].

On the other hand, stearic acid does not form stable monolayers at the air-water interface, which can be seen as a decline of the surface pressure when holding the barriers at a constant area (data not shown). Consequently, the transfer of monolayers containing stearic acid showed transfer ratios higher than 1.8.

In general, after reaction with ozone, the contact angle was very low and in some cases not even measurable due to the formation of reaction products that made the surface hydrophilic (contact angles smaller than 10° are difficult to assess). This behavior was not observed for the mixture of stearic acid:oleic acid deposited on mica, where the monolayer kept part of its hydrophobic character after exposure due to the presence of the unreacted stearic acid. In addition, the choice of the solid substrate also played a role, as discussed below. In contrast, monolayers composed of a mixture of saturated and unsaturated phospholipids formed very hydrophobic surfaces, which after reaction kept most of their hydrophobic character. Transfer ratios of 1.0 to 1.1 were obtained when transferring monolayers containing phospholipids onto solid substrates.

Regarding the solid substrates, it can be seen for all monolayers that higher contact angle values were obtained for monolayers deposited on mica compared to those deposited on silicon. This indicates that a weaker interaction is established between the headgroups of the monolayer molecules and the silicon surface, as has been previously reported[90]. It has been suggested that the structure of the silicon surface generates enough free volume[91] in the monolayer packing to permit some degree of solvation of the polar

headgroups by water[90]. However, the analysis of the differences found between samples deposited on mica and silicon was beyond the scope of this research.

Therefore, a study was devised in which DSPC, DOPC, and mixed monolayers of DSPC:DOPC (2:1), DMPC:DOPC (2:1), DMPC:DOPC (1:2), and DPPC:DOPC (2:1) were exposed for different times to ozone in similar conditions applied during the preliminary study. In addition, the monolayers were transferred at different surface pressures in order to discover how surface morphology, surface packing, and the accessibility of the double bond affect the reaction and the measured contact angle.

The transfer of monolayers, exposure to ozone and measurement of contact angles of DSPC, DOPC, and DSPC:DOPC and DMPC:DOPC binary mixtures were obtained in part by undergraduate students working under my supervision, following the experimental scheme I have previously devised. In addition, I carried out the analysis by AFM for all samples and the overall interpretation of the data.

4.3.2. Compression isotherms of studied monolayers

The compression isotherms of each monolayer were recorded with the purpose of deciding the value of surface pressure at which the transfer was going to be performed. It identified the surface phase that the monolayer presented while being transferred to mica. Binary mixtures of phospholipids were prepared using three saturated and one unsaturated symmetric phosphocholines, which contain aliphatic chains of 14 to 18 carbons. Table 1 in the experimental section presents a description of the phospholipids used, their molecular formula, scientific name and structure.

Figure 11 shows a comparative graph of the isotherm of the mixed monolayer of DSPC:DOPC (2:1), and the isotherms of the pure components. As indicated by the isotherms, DSPC exhibits a condensed phase at all surface pressure values while DOPC shows a liquid expanded phase.

Regarding the mixture, the critical area of the monolayer is observed as expected between the corresponding values of the pure monolayers[73]. A plateau is present in the isotherm of the mixture at about the surface pressure value at which pure DOPC collapses suggesting that this compound is collapsing in the mixed monolayer at this point of the compression. This also points to the fact that the two phospholipids are not miscible[92]. The collapse of DSPC is seen as a second collapse at a molecular area value lower than the required minimum area occupied by a phosphocholine molecule, which is approximately 40 Å[73], since DOPC molecules are not forming a monolayer anymore.

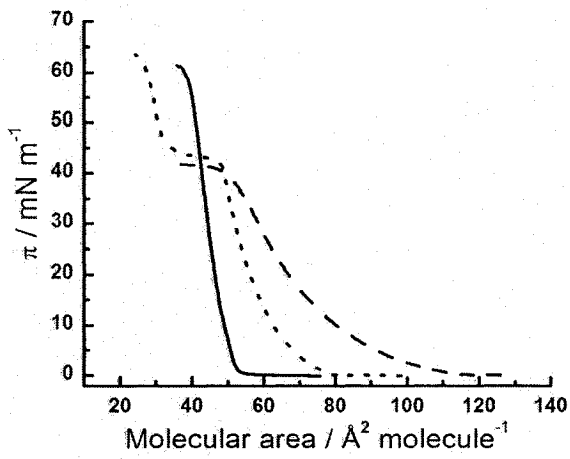

Figure 11: Compression isotherms of monolayers of DSPC (solid line), DOPC (dashed line), and DSPC:DOPC (2:1) (dotted line).

Monolayers of the mixtures of DMPC:DOPC (2:1) and DMPC:DOPC (1:2) were also characterized and compared to the corresponding pure monolayers (Figure 12). Both lipids show a liquid-expanded phase at all surface pressure values, and the same behavior is seen for the monolayers of the mixtures. DMPC is a saturated phospholipid but its aliphatic chains are shorter than those of DSPC, therefore, the cohesion and close interaction of a condensed phase is less favored. This behavior makes DMPC likely to be miscible with DOPC. However, the mixture of these two phospholipids shows a positive deviation from the ideal mixture since the critical area is higher for the isotherms of the mixtures when compared to the pure monolayers. This could be explained by the repulsive interactions brought about by the presence of unsaturations in the oleyl chains, which decreases the lateral interactions among non-polar alkyl chains.

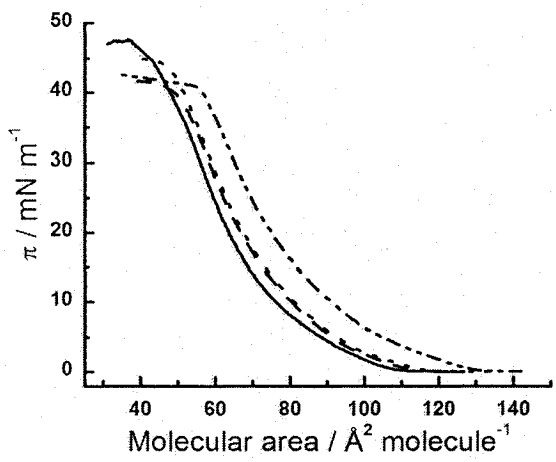

Figure 12: Compression isotherms of monolayers of DMPC (solid line), DOPC (dashed line), DMPC:DOPC (2:1) (dotted line), and DMPC:DOPC (1:2) (dashes and dots).

Since a pure DPPC monolayer undergoes a distinctive transition between a liquid expanded phase and a condensed phase during compression, a monolayer of a DPPC:DOPC mixture should experience a change in miscibility between the two phospholipids as the surface pressure increases. Both isotherms can be seen in Figure 13 together with a DOPC compression isotherm.

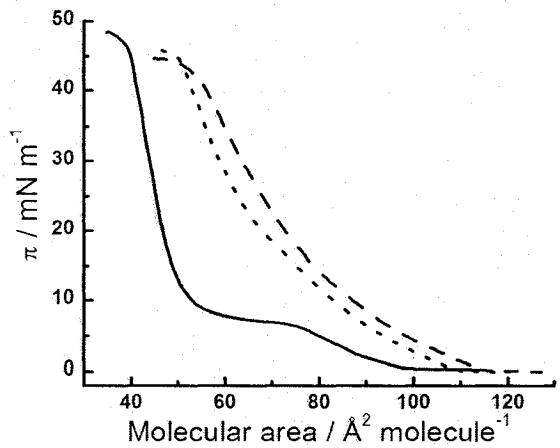

Figure 13: Compression isotherms of monolayers of DPPC (solid line), DOPC (dashed line), and DPPC:DOPC (2:1) (dotted line).

As expected, the isotherm of the mixture is located between the isotherms of the two pure monolayers, regarding molecular areas. The surface pressure steadily increases during the compression of the mixed monolayer and there is no appreciable feature in the curve confirming the existence of any phase transition or change in miscibility. Characterization by atomic force microscopy, described below, gave more information about the coexistence of DPPC and DOPC in a monolayer.

4.3.3. Analysis by atomic force microscopy of the studied monolayers

The studied monolayers were transferred to mica and examined by AFM to confirm monolayer miscibility or the existence of phase separation. A monolayer of DSPC:DOPC (2:1) was deposited on mica at 30 mN m^{-1} and at a transfer rate of 2 mm min^{-1}. The analysis of the monolayers by AFM shows clear circular domains (with an approximate diameter of 0.2 to 12 μm) of condensed DSPC surrounded by liquid-expanded DOPC. The image obtained following this procedure shows the same domains as the image shown in Figure 14 of a monolayer of the same mixture deposited on silicon.

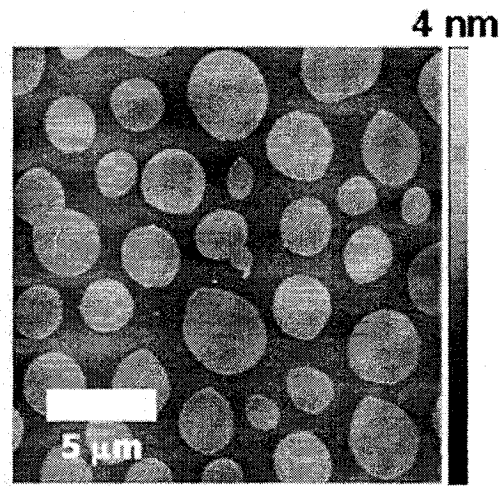

Figure 14: Image obtained by atomic force microscopy of a DSPC:DOPC (2:1) monolayer deposited on silicon after being transferred.

Domains are identified based on the characteristic phases formed by DSPC and DOPC as well as by estimating height differences between the molecules according to the corresponding chemical structures. DSPC domains were found to be 0.5 ± 0.1 nm higher

than the DOPC surrounding area. This result agrees with previously reported step height differences for the coexistence of condensed and liquid expanded phases in AFM images captured in tapping mode[93].

No phase separation was observed for either DMPC:DOPC (2:1) or DMPC:DOPC (1:2), which confirms DMPC and DOPC are completely miscible. Analysis by atomic force microscopy revealed a homogeneous surface (data not shown).

In the case of monolayers of DPPC:DOPC (2:1) deposited on mica, the coexistence of two phases was observed when transferring at 30 and 4 mN m^{-1} (Figure 15). When the monolayer is transferred at 4 mN m^{-1}, phase coexistence is observed just before the phase transition of DPPC, and although both phospholipids are nominally miscible at this point, according to the AFM image (Figure 15, *Right*) DPPC aggregates are already starting to form (lighter domains in Figure 15, *Right*). This formation of very small condensed domains of DPPC at very low surface pressures (3-5 mN m^{-1}) has been previously observed by fluorescence microscopy for both DPPC and DPPC:DOPC monolayers[94]. In addition, DPPC aggregates may be formed during the transfer to the solid substrate since these aggregates are lined up as stripes positioned perpendicularly to the direction of the transfer, which is also well known for DPPC[95]. Even though DOPC is a longer molecule than DPPC with two more carbons in its aliphatic chains, a step-height difference of 0.6 ± 0.1 nm between the DPPC condensed phase and the DOPC liquid expanded phase was observed. Likewise, the AFM image of the sample transferred at 30 mN m^{-1} shows larger domains, which is an evidence of higher DPPC aggregation

occurring as a result of monolayer compression. The height difference between phases remains the same at higher surface pressures.

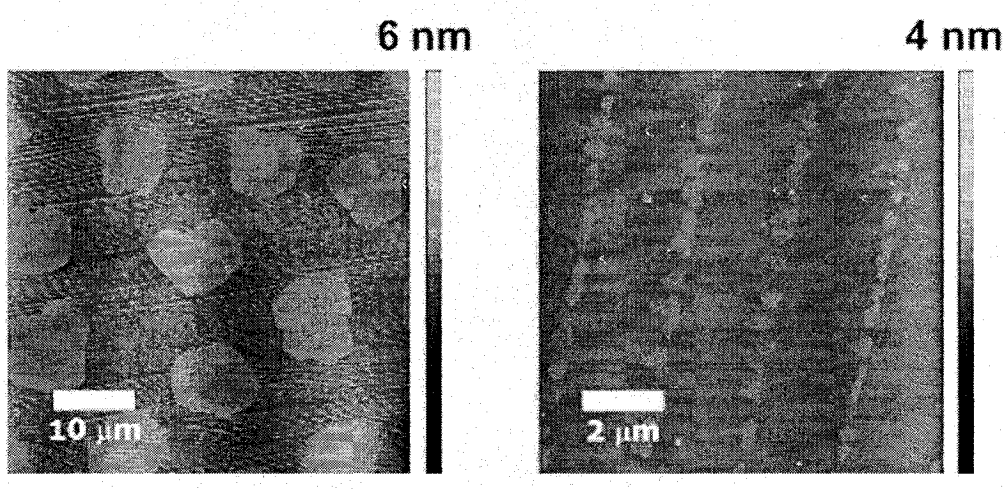

Figure 15: Height images obtained by atomic force microscopy of DPPC:DOPC (2:1) monolayers deposited on mica, at 30 mN m^{-1} (*Left*), and 4 mN m^{-1} (*Right*).

4.3.4. Ozone exposure followed by atomic force microscopy

Atomic force microscopy was used with the purpose of observing, and monitoring if possible, changes in the surface morphology of monolayers due to exposure to ozone. All monolayers were analyzed after being transferred to silicon or mica using the Langmuir-Blodgett technique. AFM images were obtained before and after exposure to high ozone concentration (> 30 ppm) for 5 minutes. The objective was to find by AFM analysis any feature present at the surface due to the exposure to ozone.

A monolayer of a single unsaturated compound, such as oleic acid, deposited on a solid substrate was observed by AFM as a homogeneous image of the surface since there are no differences in height nor detectable features at the surface (oleic acid maintains a

liquid expanded phase throughout compression). No visible feature was seen after ozone exposure either. For that reason, mixtures of saturated and unsaturated compounds were utilized to obtain appreciable height differences. However, mixed monolayers of stearic acid:oleic acid (1:1) and (2:1) were analyzed after exposure finding no visible feature in the scanned image. Both compounds have similar chain lengths but the presence of the double bond impedes a higher monolayer packing so only a liquid expanded phase is seen at any surface pressure.

In addition, these monolayers were soft and easily modified by the AFM tip, bringing also unwanted effects on the quality of the scanned image obtained (e.g. dragged material following the scan direction was observed in the images). On the other hand, mixtures of saturated and unsaturated phospholipids, when transferred to a solid substrate, were more stable and less prone to be affected by the AFM tip[96]. This stability, together with the possible occurrence of phase coexistence, should make height differences possible to be detected[93], and potentially help to observe the outcome of the reaction in the AFM images.

Monolayers of DSPC:DOPC (2:1) showed phase separation, as seen in Figure 14, in which lighter domains comprise the DSPC condensed phase and the darker surrounding is the DOPC liquid expanded phase. After being exposed to ozone at high concentration for 5 min, it is possible that rearrangements occurred at the surface (Figure 16, *Left*) because of DOPC being cleaved by ozone. These rearrangements occur because the monolayer molecules are physisorbed to the solid substrate and not chemically attached.

The majority of the main reaction products are expected to remain at the surface, with the exception of nonanal as was mentioned before. Moreover, no significant variation was found for the step-height difference between phases. The phase image of the same monolayer (Figure 16, *Right*) is also useful for imaging of the surface as the fluidity of the molecules at the surface differed (since DSPC is in a condensed phase and DOPC in a liquid expanded phase).

Monolayers of DMPC:DOPC (2:1) did not show any phase separation, or any visible change due to the reaction (data not shown) since the homogeneity of the surface prevents any morphological change to be seen.

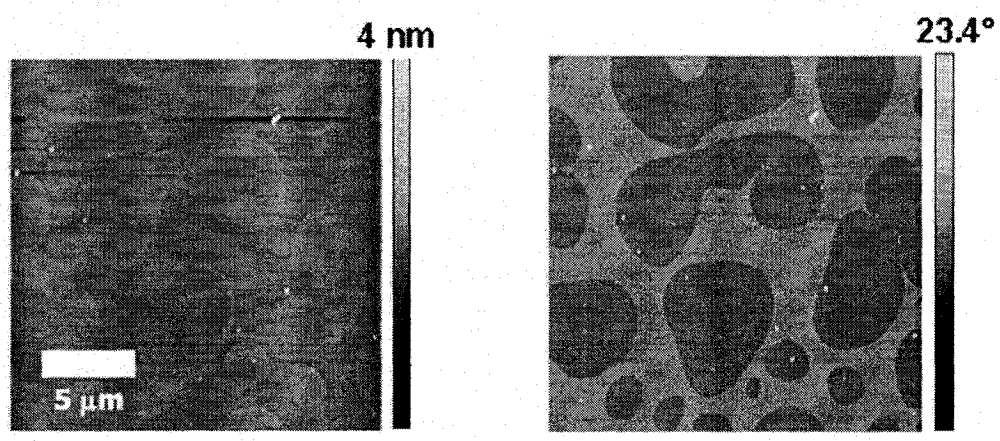

Figure 16: Images obtained by atomic force microscopy of the DSPC:DOPC (2:1) monolayer deposited on silicon shown in Figure 14, after exposure to ozone (> 30 ppm) for 5 minutes: height image (*Left*), phase image (*Right*).

Still, the detected changes in the images obtained are difficult to assess and quantify despite ellipsometry measurements suggesting that a slight decrease in average thickness of the film (decreased by approximately 0.1 nm, data not shown) took place as

a consequence of the exposure for samples of both DSPC:DOPC (2:1) and DMPC:DOPC (2:1).

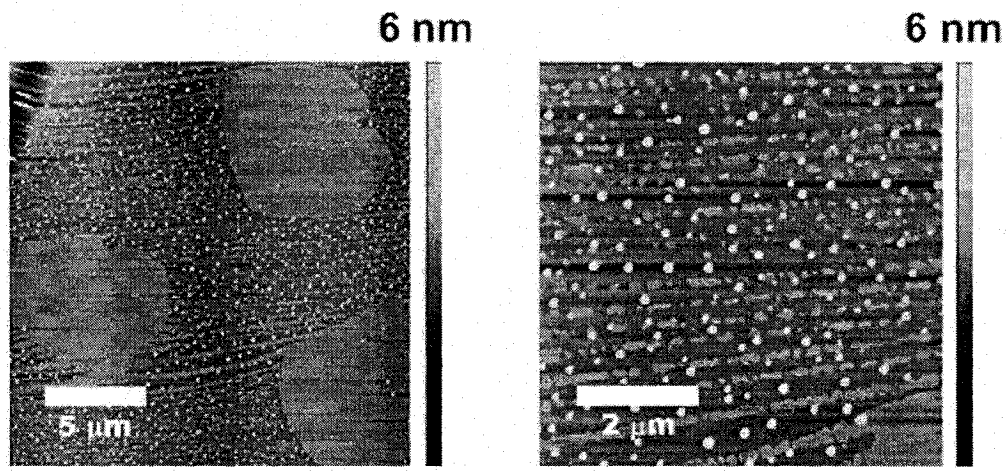

Figure 17: Images obtained by atomic force microscopy of the DPPC:DOPC (2:1) monolayer deposited on mica at 30 mN m^{-1} shown in Figure 14, *Left*. This sample was exposed to ozone (> 30 ppm) for 5 minutes: an image corresponding to a 20 µm scan (*Left*) and a zoomed image (*Right*) are shown.

Monolayers of DPPC:DOPC (2:1) deposited on mica were exposed to ozone as well (Figure 17). Aggregated structures of sizes ranging from 3 to 9 nm were observed. Similar structures were observed as well in AFM images of processed monolayers of DSPC:DOPC (2:1) and DMPC:DOPC (2:1). A previous report has found similar organic formations during the ozonolysis of self-assembled monolayers of vinyl-terminated compounds on silicon substrates by using AFM imaging[97]. These results are explained by a possible polymerization induced by the Criegee intermediate. However, a thorough spectroscopic study of the composition of such aggregates formed from the DPPC:DOPC

(2:1) monolayer would be necessary to extend the same explanation to this system. On the other hand, no significant variation of the step height difference between liquid expanded and condensed phases before and after reaction was observed either. Hence, a further study by AFM of the ozonolysis of these systems was not carried out.

4.3.5. Ozone exposure followed by contact angle measurements

The monolayers of DSPC:DOPC (2:1) were deposited on mica at surface pressure values of 10 and 30 mN m^{-1} before exposure to ozone. Monolayers of the DMPC:DOPC mixtures were also transferred to mica but at a pressure of 25 mN m^{-1} since at 30 mN m^{-1} some collapsed material was already seen. As the surface pressure was less stable before transferring for DMPC:DOPC monolayers, compared to DSPC:DOPC monolayers, the transfers were performed at a faster rate of 5 mm min^{-1} to improve transfer quality.

Figure 18 shows the change in contact angle ($\Delta\theta$) with time of exposure to ozone for monolayers of DSPC, DOPC and DSPC:DOPC (2:1). The contact angle value at 0 min of exposure time corresponds to the standard sample transferred and measured like the rest of the samples but not exposed to ozone. Therefore, the value obtained accounts for the normal variation of the contact angle with time between the first and the second measurements. For each point, the graph shows error bars that correspond to the variation between samples exposed to ozone at a specific time. The study of the effect of the ozone exposure of pure DSPC and DOPC monolayers was performed by undergraduates and repetitions were not available for all time points. However, the error was estimated to be ± 3° based on repetitions of the exposure of DSPC:DOPC (2:1) monolayer samples to

ozone for 5 min. The focus of the study was on the exposure of mixed monolayers for which error bars have been included.

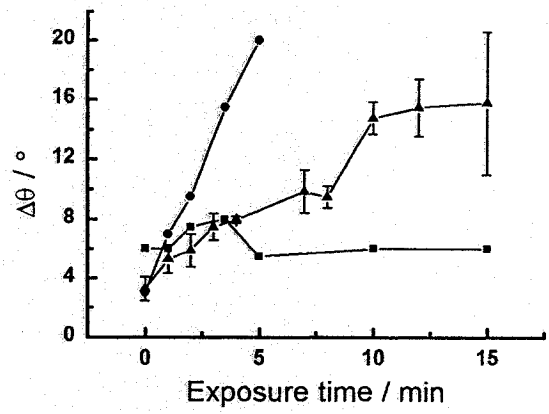

Figure 18: Change in contact angle due to exposure to ozone for monolayers of DSPC (■), DOPC (●), and DSPC:DOPC (2:1) (▲). All samples were transferred at 30 mN m^{-1}.

The contact angle of water with a monolayer of DSPC deposited on mica was measured before and after exposure to ozone for up to 15 minutes. The variation measured was found to be within experimental error and confirmed that the monolayer of DSPC does not react with ozone since no unsaturation is present. A similar determination was performed with a monolayer of DOPC and a significant variation was observed as the time of exposure was increased. This confirms the loss of the hydrophobic character of the surface as it is processed. In the case of the mixture, the exposure to ozone also showed an increase of the contact angle but at a slower rate than for a monolayer of DOPC since part of the monolayer remained hydrophobic after reaction. The results

prove that contact angle measurements can be used to follow the reaction of ozone with unsaturated phospholipids.

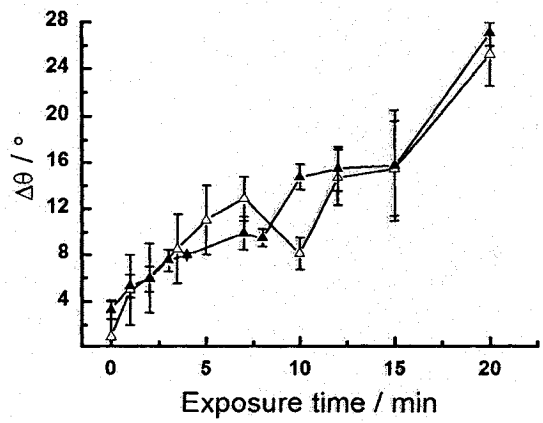

Figure 19: Comparison of the variation of the contact angle with exposure to ozone for monolayers of DSPC:DOPC (2:1) deposited at 10 (△) and 30 mN m^{-1} (▲).

Monolayers of DSPC, DOPC and DSPC:DOPC (2:1) transferred at 10 mN m^{-1} were also exposed to ozone in order to investigate the effect of surface coverage on the reaction. After exposure, a similar trend is observed for the variation of the contact angle with time for monolayers of DSPC:DOPC (2:1) transferred at different surface pressures (Figure 19). Similar results were found for pure monolayers of DSPC and DOPC (data not shown) which did not show surface pressure dependence either. These findings agree with computer simulations data and experimental results obtained by Wadia *et al.*[43], which found that the yield of gas-phase products of the reaction of OPPC monolayers with ozone was independent of the molecular area. Computer simulations suggested that

the similarities between the chemical environments around the double bond at different compressions were the reason for this non-dependence.

The immiscibility of DSPC and DOPC leads to the formation of a phase-separated mixture at both 30 and 10 mN m^{-1}. This means that after the reaction of the monolayer with ozone, hydrophobic DSPC domains remain on the surface surrounded by a hydrophilic media. The possible effect of the surface morphology and surface patterning on the measurement of the contact angle[84] was tested by depositing monolayers of DMPC:DOPC (2:1) on mica which were further exposed to ozone.

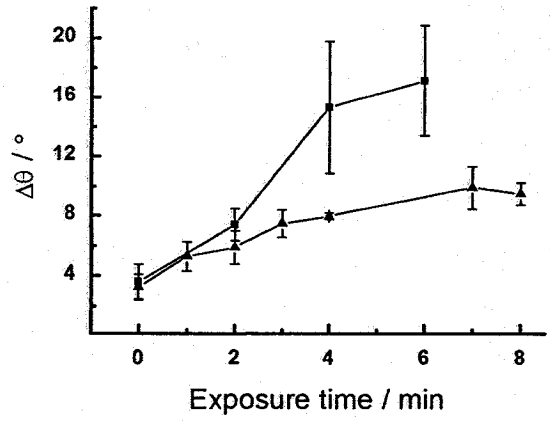

Figure 20: Comparison of the variation of the contact angle with exposure to ozone for monolayers of DSPC:DOPC (2:1) (▲), transferred at 30 mN m^{-1}, and DMPC:DOPC (2:1) (■), transferred at 25 mN m^{-1}.

As seen in Figure 20, a larger change in the hydrophobic properties of the surface (characterized by $\Delta\theta$) with increasing exposure time is observed for monolayers of DMPC:DOPC (2:1) when compared to the exposure of DSPC:DOPC (2:1) samples. This

result suggests that the hydrophobic domains of DSPC found in the phase-separated DSPC:DOPC (2:1) surface influence the measurement of the contact angle, when compared to measurements on the homogeneous surface of DMPC:DOPC (2:1) monolayers. This agrees with reports in the literature that the hydrophobic character of an already hydrophobic surface increases as a result of the presence of surface defects[84], either due to the air trapped below the drop (Cassius-Baxter approach) or by an increase of the hydrophobic surface area in contact with the water (Wentzel approach)[98,99] (Figure 21). In general, the processing of DOPC molecules would make the surface more hydrophilic. However, this effect would be less pronounced due to the presence of phase separation, complicating a kinetic interpretation of the results. In a phase separated DSPC:DOPC monolayer, DSPC domains are higher than the surrounding DOPC and this structure approximates the schematic representation of a surface shown in Figure 21.

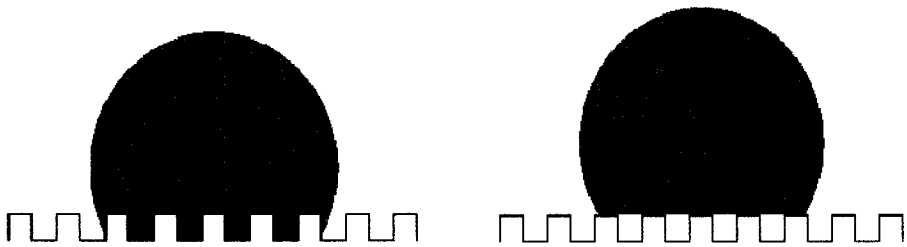

Figure 21: Representation of Wentzel (*Left*) and Cassius-Baxter (*Right*) approaches to the wetting of a solid surface by a drop of a liquid (based on reference 81).

For instance, Wentzel approach explains how the measured contact angle, or "apparent" contact angle, differs from the "true" contact angle due to the effect of the roughness of the surface[84]. The "true" contact angle would be that measured if the surface had no irregularities or if it were highly polished. The aqueous drop is assumed to be completely wetting the solid surface; therefore, the presence of irregularities on the surface would affect the actual surface area in contact with the water. On a not well-wetted, mostly hydrophobic surface, this is observed as an increase of the measured contact angle, also confirming the dependence of the contact angle on the composition and chemical heterogeneity of the sample.

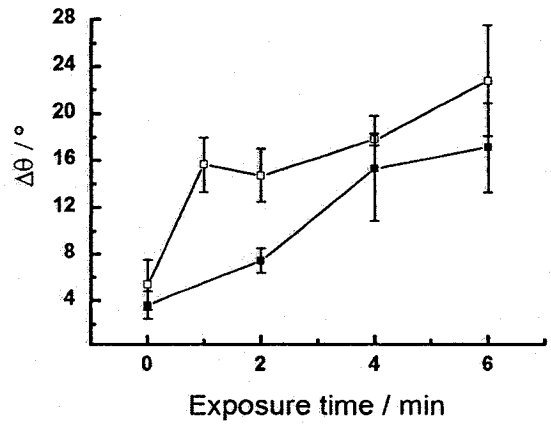

Figure 22: Comparison of the variation of the contact angle with exposure to ozone for monolayers of DMPC:DOPC (2:1) (■) and DMPC:DOPC (1:2) (□).

In the case of the monolayer of DMPC:DOPC (1:2), with a larger unsaturated composition, a larger change of the contact angle is seen at any given time (Figure 22), which is consistent with the fact that more reaction sites for ozone are found in the

surface and its hydrophobicity is lower after the reaction. However, this hydrophobic character of the surface changes at the same rate for both mixtures of DMPC and DOPC.

In order to confirm the effect of the surface morphology on the measurement of the contact angle, monolayers of DPPC:DOPC (2:1) were also studied. As DPPC undergoes a phase transition from a liquid expanded to a condensed phase, the compression of the mixture with DOPC revealed both phase coexistence and miscibility at different stages of the isotherm. Phase coexistence was observed by AFM for samples transferred at 10 mN m^{-1}. Therefore, the transfers at a lower surface pressure value were made at 4 mN m^{-1} in order to observe a homogeneous surface of both DPPC and DOPC in a liquid expanded phase. Still, AFM images showed some DPPC aggregation. Hence, in order to avoid as much aggregation as possible these transfers were performed at a higher subphase temperature of 30°C, since the surface pressure at which the phase transition takes place increases with an increase in temperature[100]. AFM images of samples transferred at 30°C showed the surface was not completely homogeneous but exhibited much less aggregation.

Figure 23 shows the results of the exposure to ozone for these monolayers. Both curves obtained for monolayers of DPPC:DOPC (2:1) transferred at different surface pressures, with more or less DPPC aggregation, show the same rate of change of hydrophobicity with ozone exposure.

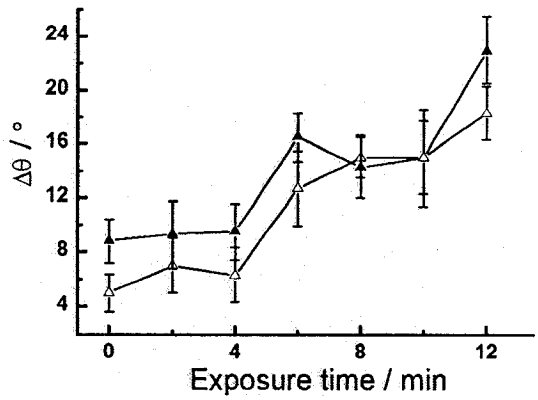

Figure 23: Comparison of the variation of the contact angle with exposure to ozone for monolayers of DPPC:DOPC (2:1) deposited at 4 (△) and 30 mN m^{-1} (▲). Samples deposited at 4 mN m^{-1} were transferred at a subphase temperature of 30°C.

Contrary to what was initially expected, similarities can not be found between the exposure of DPPC:DOPC (2:1) monolayers to the exposure of DSPC:DOPC (2:1) and DMPC:DOPC (2:1) monolayers (Figure 20). Still, the observed rate for the variation of the contact angle for DPPC:DOPC (2:1) is closer to that of the DSPC:DOPC (2:1) mixture. This could be explained as a consequence of also having phase coexistence and similar height differences between the lipids forming the mixture. However, DSPC seems to aggregate more than DPPC as the latter forms less condensed phase domains on the surface (for comparison, see Figure 15 for DPPC:DOPC (2:1) and Figure 14 for DSPC:DOPC (2:1)).

Overall, it can be concluded that the processing of organic monolayers by ozone can be followed by measuring how the hydrophobic character of a surface decreases.

However, the determination depends highly on the morphology of the surface, which is directly associated with the composition of the deposited monolayer and the presence of phase coexistence. In addition, this determination does not permit a real-time monitoring of the reaction. Other techniques of surface analysis, such as atomic force microscopy and ellipsometry, provide useful information on the characteristics of the surface being modified but do not supply quantitative results to analyze the reaction. Nevertheless, the analysis by atomic force microscopy of exposed monolayers with mixed composition revealed rearrangements taking place at the surface due to the reaction. It also suggests the presence at the surface of residual reaction products since height changes between phases are not observed.

4.4. Pendant drop experiments

4.4.1. Introduction

The spreading and formation of a monolayer on the surface of a pendant drop together with the application of ADSA brings the possibility of recording values of surface tension as achieved on a film balance. The pendant drop proxy allows the use of lower subphase volumes, which consequently facilitates the building of a suitable setup for putting in contact a surface film and a constant flow of ozone, or any other gas. The outcome of the reaction is registered as a change in surface tension, and makes possible to relate this surface specific variable exclusively to the changes in concentration of the reactant located at the surface. In contrast to the Langmuir-Blodgett system described in the previous section, the application of ADSA to the pendant drop permits a real-time

monitoring of the reaction. This offers a new approach to the processing of surface films and permits the study of the kinetics of the reaction.

4.4.2. Monolayer compression on a pendant drop

The spreading of surfactants directly on a pendant drop is a recently developed procedure that has been applied for studying interactions in lipid-lipid and lipid-protein systems[101]. Two methods for spreading surfactants at the surface of a pendant drop have been described in the literature according to the way the solution is released from the syringe to the drop surface[102,103], namely on-capillary deposition (also called surface deposition), and on-drop deposition (or bulk deposition). The last two methods were tried in order to determine which one to use.

On-capillary deposition is performed by releasing from the syringe the solution while touching the capillary just above the drop. Then the solution runs down the capillary to cover the whole drop surface. In the on-drop deposition, the solution to spread is released while the syringe is touching the drop surface. After releasing the content of the syringe, the amphiphilic molecules spread out and coat the surface of the drop. For long-chain amphiphiles, the amount of dissolution into the subphase can be considered negligible[102]

Compression isotherms of DPPC were obtained after spreading and compared to the isotherm obtained on a Langmuir trough. DPPC was selected as the standard compound for these experiments since its isotherm presents a characteristic phase transition from liquid expanded to condensed phase.

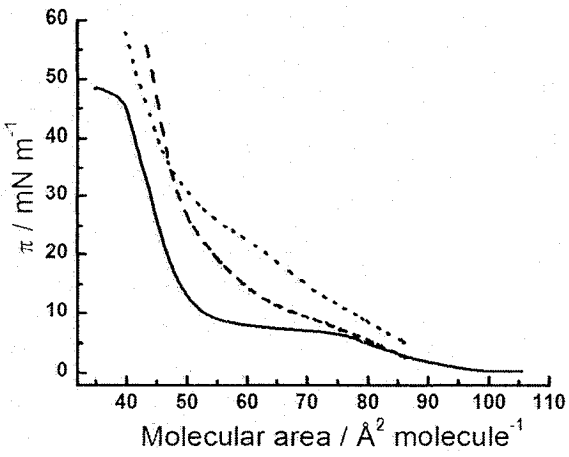

Figure 24: Comparison between compression isotherms of DPPC obtained by different spreading methods on a pendant drop: on-drop deposition (dashed line), on-capillary deposition (dotted line), at a compression speed of 0.02 $Å^2$ $molecule^{-1}$ s^{-1}. Solid line corresponds to an isotherm obtained on a Langmuir film balance (compression speed was 0.12 $Å^2$ $molecule^{-1}$ s^{-1}).

Figure 24 shows the results of the comparison of the two spreading methods. On-drop deposition was applied in our experiments as this method yielded the best agreement between compression isotherms of DPPC spread on the drop surface and those obtained using a traditional Langmuir film balance. The differences between isotherms obtained on the surface tensiometer with respect to those obtained on a Langmuir trough have been well described in the literature for DPPC[102]. Differences have been attributed to the sensitivity of handling small amounts of the solution to spread and the possible formation of micelles below the surface[102].

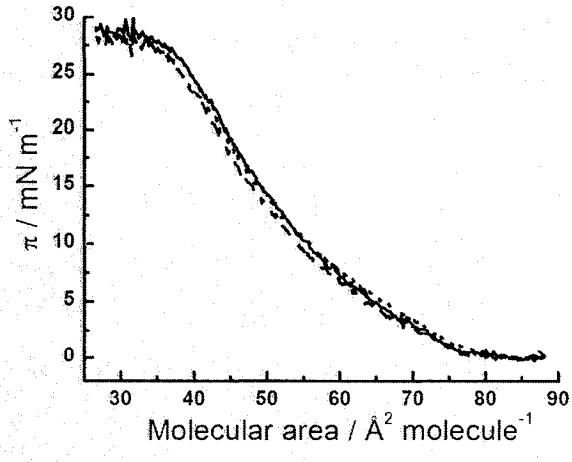

Figure 25: Compression isotherms of oleic acid monolayers on a pendant drop at different compression speeds: 0.13 $Å^2$ $molecule^{-1}$ s^{-1} (solid line), 0.07 $Å^2$ $molecule^{-1}$ s^{-1} (dashed line), and 0.02 $Å^2$ $molecule^{-1}$ s^{-1} (dotted line).

Finally, Figure 25 shows the result of a study of the effect of the compression speed in drop experiments. Oleic acid monolayers were tested finding no difference in the range from 0.02 to 0.13 $Å^2$ $molecule^{-1}$ s^{-1}.

4.4.3. Ozone exposure of a monolayer deposited on a pendant drop

A visible decrease on the value of the surface pressure was observed when exposing an oleic acid monolayer to ozone (as shown in Figure 26, *Left*. See also experimental section). Likewise, a monolayer of stearic acid was exposed to ozone (Figure 26, *Right*) following similar experimental conditions and no changes occurred to the surface pressure of the monolayer. Since stearic acid is a fully saturated fatty acid, this confirmed that the changes in the surface pressure were due to the degradation of the

surface layer resulting from the reaction of ozone with the double bond of the oleic acid molecule.

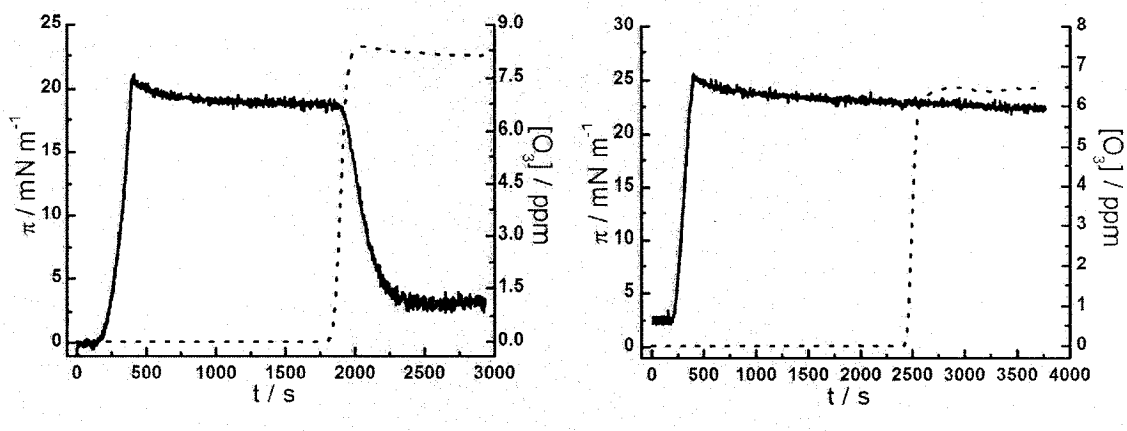

Figure 26: Exposure to ozone of a monolayer spread on the surface of an aqueous drop (initial surface area 0.4 cm^2): surface pressure π (solid lines), ozone concentration (dashed line). The mixture of ozone and air was flowed at 100 cm^3 min^{-1}. The monolayer was deposited using 0.6 to 0.8 μL of a 0.1 mM spreading solution in $CHCl_3$ of oleic acid. *Left*: oleic acid. *Right*: stearic acid.

The decrease in surface pressure ended at values close to zero suggesting that the final products of the reaction have low surface activity. Isotherms of nonanoic acid and nonanal, which are expected reaction products, were obtained as part of this study. They did not show any appreciable surface pressure throughout compression on a Langmuir trough or in the pendant drop. While the difunctional reaction products are even less surface active, the effect of the possible formation of high molecular products[51] was not noticeable. Furthermore, Voss *et al.* concluded that for drop diameters greater than 1.2 μm the oxidation products should be fully soluble[65].

The measured decrease of surface pressure π has to be converted into values of oleic acid concentration at the surface $[Oleic]_{surf}$ to make possible any kinetic analysis. An equation of state for the monolayer, analogous to that for an ideal gas in a three dimensional system, describes this relationship[72]:

$$\pi A = RT \quad (4)$$

where π is the surface pressure, R is the gas constant, T is the temperature, and A is the area per mole of a compound at the surface (inversely proportional to surface concentration). For the purpose of this study, the surface concentration of oleic acid represents the amount of oleic acid actually present at the surface per unit area of the interface, and it is expressed here as the oleic acid concentration at the surface $[Oleic]_{surf}$.

A common π - area isotherm for an oleic acid monolayer can be transformed into a π - $[Oleic]_{surf}$ isotherm since the exact volume of oleic acid solution spread at the surface is known as well as the concentration of the solution. The π - $[Oleic]_{surf}$ relationship shows linearity for a limited range of surface concentrations, therefore, it is calculated by fitting a plot of $[Oleic]_{surf}$ versus π to a polynomial equation as shown in Figure 27. Thus, an equation is obtained in which a value of oleic acid concentration at the surface is related to each measured value of surface pressure. However, this relationship is not applicable above 30 mN m^{-1} since the monolayer has already collapsed. It is not applicable either for oleic acid concentrations for which no surface activity is observed (when $\pi = 0$ and the monolayer is in a gas phase-like state).

This approach has been previously applied in protein adsorption studies[104] for which the speed of compression used avoids desorption and surface equilibrium is achieved. Both conditions are also satisfied when compressing an insoluble monolayer like that formed by oleic acid.

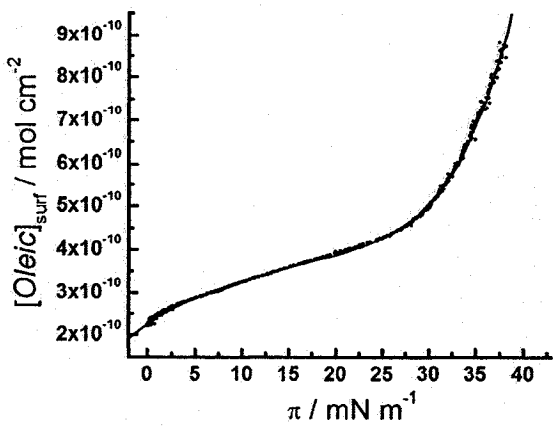

Figure 27: A plot of oleic acid concentration at the surface $[Oleic]_{surf}$ versus surface pressure π (●) is fitted to a polynomial function (solid line), $R^2 = 0.99$.

There is no significant effect of cooling of the drop surface expected due to evaporation on the monolayer properties. The temperature differences between bulk and surface reported for aqueous subphases range from 0.25 K for a Langmuir trough with monolayer coverage[105] to 4.5 K for a pendant drop with no monolayer coverage[106]. Within this range (291-296 K) the surface pressure-area isotherm of oleic acid exhibits only minor differences (about 8 $Å^2$ $molecule^{-1}$) in critical area. These differences are comparable to a maximal change in concentration of the spread solution of less than 0.03 mM.

Finally, the application of this approach, in which a π - $[Oleic]_{surf}$ relationship is obtained, is feasible for the system studied since oleic acid is the only surface active species at the air-water interface during the progress of the experiment. In the case where more than one component of a mixture or any of the reaction products are also appreciably surface active the analysis is more complicated. Thus, the study of the processing of such a complex monolayer would need to be preceded by a thorough study of compression isotherms of mixed monolayers composed by all surface active compounds involved.

4.4.4. Kinetic analysis of the reaction

The flow of ozone into the reaction chamber is steady at all times, therefore the ozone concentration is assumed to be constant. This is the basis for the pseudo-first order reaction premise that permits the calculation of the corresponding pseudo-first order rate constant k'. If $k'=k_2[O_3]$, then the reaction rate is expressed as:

(5) $$-\frac{d[Oleic]_{surf}}{dt} = k'[Oleic]_{surf}$$

Solving equation (2):

(6) $$\ln[Oleic]_{surf} = k't + \ln[Oleic]_{surf_0}$$

therefore, the rate constant k' can be calculated from the plot of $\ln[Oleic]_{surf}$ versus time t.

Figure 28 shows a closer examination of the obtained data plot for the exposure of oleic acid to ozone. A plot of $\ln[Oleic]_{surf}$ versus t is linear in the range limited by the arrows, which is characteristic of pseudo-first order kinetics. Pseudo-first order behavior

is not observed for the initial points of the surface pressure change suggesting that ozone has not reached yet a steady-state concentration and therefore these were not taken into account for further calculations.

Close to the end of the reaction, the surface pressure is no longer solely a function of $[Oleic]_{surf}$. In addition, the estimation of $[Oleic]_{surf}$ is limited to the range of concentrations covered by the compression isotherm (used for the validation of the π - $[Oleic]_{surf}$ relationship) for which the surface pressure is detectable, namely throughout the liquid-expanded phase. Thus, data points located after the second arrow on the graph were not included in the calculation of the rate constant.

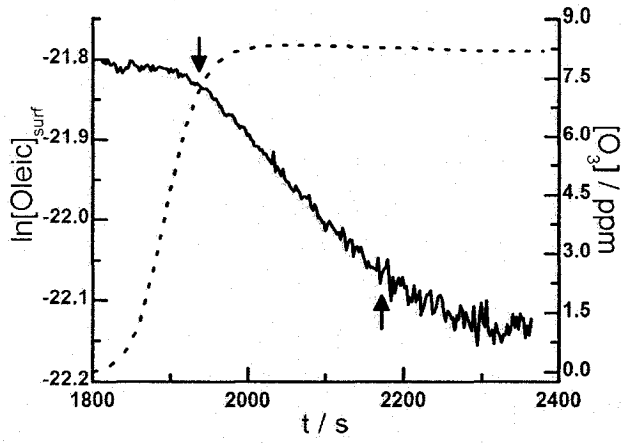

Figure 28: Exposure to ozone of a monolayer spread on the surface of an aqueous drop (initial surface area 0.4 cm^2) showing $ln[Oleic]_{surf}$ (solid line) and ozone concentration (dashed line) as a function of time. Arrows indicate region for which pseudo first-order kinetics were observed.

A summary of the results of experiments in which monolayers of oleic acid were exposed to different concentrations of ozone is presented in Table 4. Values presented are the average of at least three experiments while error values represent 2σ.

Table 4: Values of the pseudo-first order rate constant k' obtained for different ozone concentrations.

$[O_3]$ (ppm)	$[O_3] \times 10^{12}$ (molecules cm^{-3})	$k' \times 10^{-3}$ (s^{-1})
25	615	5.5 ± 0.2
19	467	4.4 ± 0.1
15	369	3.8 ± 0.2
8	197	1.4 ± 0.4
5	123	1.2 ± 0.1
2	49	0.4 ± 0.4
0.3	7	0.02 ± 0.02

Figure 29 shows the graph obtained when plotting k' versus $[O_3]$. A good correlation ($R^2 = 0.98$) shows that the data obtained is consistent with the assumption of the pseudo-first order kinetics for the reaction, and supports the fact that the proportionality of the measurements of surface pressure to the extent of the surface reaction can be used for studying the kinetics of the reaction. The second-order rate constant k_2 is obtained from the slope of this graph, being $(9.4 \pm 0.5) \times 10^{-18}$ cm^3 $molecule^{-1}$ s^{-1}.

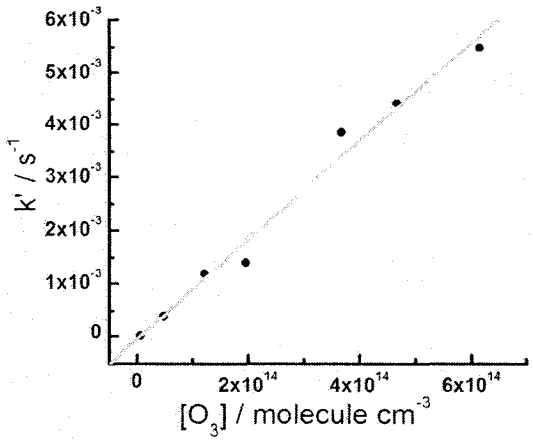

Figure 29: Plot of the values of the pseudo-first order rate constant *k'* and the ozone concentration [O_3]; linear regression of data points is included.

To estimate the surface-specific rate constant k_2^{surf} it is necessary to specify a value for the depth of ozone diffusion into the surface monolayer. Recent computer simulations have described the density profile of ozone within the surface layer for different systems including a monolayer at the air-water interface[107], and from these results it can be safely proposed that the ozone molecule would be found only at depths less than the length of an oleic acid molecule. If this length is estimated to be 1.90 nm a value of 4.9×10^{-11} cm^2 molecule^{-1} s^{-1} is found for k_2^{surf}.

4.4.5. Comparison to previous experiments found in the literature

The uptake of a gas molecule by a liquid phase is determined by several processes or transformations such as the diffusion of the gas species through the gas phase to the surface, the adsorption or desorption at the surface, the incorporation and solvation of the gas into the bulk of the liquid phase or the reaction either at the surface or in the bulk[6,55].

As explained in the second chapter of this thesis, these interactions are commonly represented by using an electric circuit resistance model in which each process, exemplified by an individual resistance, is considered to be independent of the others[6,55]. The combination of the individual resistances, either in series or in parallel, stands for the net uptake coefficient γ of the gas by the liquid phase, in which the mass-transfer rate of gas to the liquid phase is normalized to the rate of collisions of the gas molecules with the surface[6,55]. Thus, measurable parameters such as the Henry's law solubility of the gas, the mass accommodation coefficient α, and the rate of the reactions in the liquid phase and at the surface, can be used to determine γ. This variable is commonly represented as a measured uptake coefficient γ_{meas} since different proxies have been used to estimate its value.

This coefficient has been usually described in terms of the loss of the gas-phase species. However, Worsnop *et al.*[54] showed that the rate of change of the concentration of oleic acid, [*Oleic*], can also be expressed using the measured uptake coefficient for ozone:

$$\frac{d[Oleic]}{dt} = -\frac{3}{a}\frac{n_0 \bar{c} \gamma_{meas}}{4} \quad (7)$$

where γ_{meas}, is defined as the probability that the collision of an ozone molecule with an aerosol particle leads to reaction, n_0 represents the bulk concentration of ozone, a is the radius of the aerosol particle, and $\bar{c}$ is the mean kinetic speed of ozone molecules in the gas phase (calculated to be 3.9×10^4 cm s^{-1})[108].

Using this model and assuming that the limiting loss process of ozone is the reaction with oleic acid, the uptake of ozone can be represented as the sum of individual processes (resistances in the electric circuit model explained above) representing the reaction at the surface (Γ_{surf}) and the reaction in the bulk (Γ_{bulk})[47]:

(8) $$\gamma_{meas} = \Gamma_{surf} + \Gamma_{bulk}$$

Since in our experiments the amount of oleic acid in the bulk can be neglected, it is more appropriate to describe the uptake of ozone as dominated by the reaction at the surface ($\gamma_{meas} = \Gamma_{surf}$). An expression for the measured uptake coefficient at the surface was described by Smith *et al.*[47]:

(9) $$\gamma_{meas} = \Gamma_{surf} = \frac{4HRT\delta}{\bar{c}} k_2^{surf} [Oleic]_{surf}$$

where H is the Henry's law solubility constant of ozone (0.48 M atm^{-1})[47], R is the gas constant (0.0821 atm M^{-1} K^{-1}), T is the temperature (296 K), δ is the thickness of the surface layer, and k_2^{surf} is the second order rate constant (see above). Since $[Oleic]_{surf}$ is determined from the measured data, and k_2 is known (and $k_2 = \delta k_2^{surf}$), the final equation for calculating γ would be:

(10) $$\gamma_{meas} = \Gamma_{surf} = \frac{4HRT}{\bar{c}} k_2 [Oleic]_{surf}$$

This approach leads to a value of $(2.6 \pm 0.1) \times 10^{-6}$ for γ.

However, given the characteristics of the drop, which has a larger surface area than a real aerosol particle, there could be a significant contribution to the uptake from the gas diffusion of ozone. The transport of ozone molecules from the gas phase to the

surface is determined by the Knudsen number K_n which is defined as the ratio of the mean free path of the gas λ to the particle radius a[55]. The mean free path is defined as follows:

$$\lambda = \frac{3D_g}{\bar{c}} \quad (11)$$

where D_g is the gas-phase diffusion coefficient of the gas phase species involved. So far, there is no report in the literature of a direct measurement of the ozone diffusion coefficient in air[109], although 0.6 cm^2 s^{-1} could be used according to an experimental estimation[110].

Assuming a spherical geometry for the pendant drop, the same drop radius of 0.13 cm is calculated for all experiments. A Knudsen number of 0.0004 is thus obtained, which confirms that the flow of ozone to the surface is in the continuous regime[6,111], indicating that the uptake coefficient may require correction.

In order to calculate the contribution of the gas diffusion, an approximated equation could be described, based on a similar equation for nonreactive uptake[55]:

$$\frac{1}{\gamma_{meas}} = \frac{1}{\Gamma_{diff}} + \frac{1}{\Gamma_{surf}} \quad (12)$$

The measured uptake γ_{meas} would be expressed in terms of the gas-phase diffusion resistance Γ_{diff} and Γ_{surf}, a corrected variable for the reaction at the surface. The latter would represent a reactive uptake coefficient in assumed conditions of no influence or contribution from the gas-phase diffusion.

The contribution of the gas-diffusion can be calculated using the following empirical equation[55]:

$$\frac{1}{\Gamma_{diff}} = \frac{0.75 + 0.283K_n}{K_n(1+K_n)} \quad (13)$$

A value of 1874 is found for $1/\Gamma_{diff}$ which does not affect significantly the value obtained for Γ_{surf}. It can be said then that although the rate of ozone diffusion to the surface is small, the rate at which the reaction takes place at the surface is even slower, so the diffusion step is not limiting.

The quantification of the uptake of ozone by oleic acid, or any other unsaturated compound, has been carried out using different proxies and laboratory setups. Table 5 shows a comparison of γ values reported in the literature. Higher values are reported for studies in which the reaction was carried out using bulk liquids (frozen or non-frozen) and generated particles. In these proxies, the obtained result evaluated more than one process taking place and contributing to the uptake. In other words, these proxies make difficult to separate the term representing the reaction at the surface from other contributing processes such as the diffusion of the gas into the bulk of the proxy or the reaction occurring at the bulk. The approach reported here permits a simplification of the above mentioned circuit resistance model in order to quantify the contribution of the reaction at the surface to the value of the uptake, without competition from any other reactive process. This explains the lower γ value obtained when comparing to other proxies of the table also using oleic acid, either as a generated particle or as a liquid bulk.

Table 5: Values of the measured uptake of ozone reported in the literature and obtained in the current study.

		γ	proxy
Morris *et al.*[49]	2002	1.6×10^{-3}	Oleic acid generated particle
Hearn *et al.*[45]	2005	1.4×10^{-3}	Oleic acid generated particle
Moise *et al.*[42]	2002	8.3×10^{-4}	Liquid oleic acid on rotating flow tube
		5.2×10^{-5}	Frozen oleic acid
Thornbery *et al.*[58]	2004	8.0×10^{-4}	Liquid oleic acid on rotating flow tube
		7.1×10^{-4}	Frozen oleic acid
Dubowsky *et al.*[39]	2004	10^{-6} to 10^{-5}	Terminal alkenes on self-assembled monolayer
Mmereki *et al.*[64]	2003	7×10^{-8}	Anthracene adsorbed at air/water interface
McNeill *et al.*[63]	2007	$\sim 10^{-5}$	Mixed NaCl/sodium oleate generated particle
Current study	2007	2.6×10^{-6}	Oleic acid monolayer spread on drop surface

For surface film proxies, a Langmuir-Hinshelwood mechanism has been proposed[39,64,67] in which ozone is first rapidly adsorbed at the surface followed by a slow reaction between both species at the surface. This mechanism is neither indicated nor contradicted by our data. The reaction in our study was most likely carried out within the ozone concentration regime for which a linear relationship between the rate constant k' and $[O_3]$ is expected, and before reaching the plateau representing the saturation of adsorption sites. It can be seen that the ozone concentrations used here are an order of

magnitude below those at which linearity is lost as a result of the saturation of surface sites for ozone adsorption according to research carried out for reaction with PAHs at a monolayer coated surface[64,67] (ozone concentrations higher than 2×10^{15} molecule cm^{-3}).

As the spatial arrangement of both a SAM and an oleic acid monolayer at a surface pressure of about 20 mN m^{-1} is similar, our uptake values are comparable to the initial uptake values reported by Dubowsky *et al.* (10^{-6}) for equivalent ozone concentrations using a proxy comprising SAMs of terminal alkenes. Previous molecular dynamics simulations[107] have revealed the liquid-like characteristics of an unsaturated organic monolayer in which the double bond can be considered to be in the interior of an organic medium. Hence, the unsaturation being located at different positions on the alkyl chain indicates a difference in accessibility to the double bond. Vieceli *et al.* calculated the percentage of the total accessible surface area that is due to double bonds as 99.7% for a SAM of 1-octenethiolate molecules adsorbed on a gold surface[107] in contrast to 3.7% reported for a monolayer of 1-oleoyl-2-palmitoyl-sn-glycero-3-phosphocholine (OPPC) spread on a liquid surface[43]. However, similar results on the two experimental systems reassert the significance of considering the residence time of the ozone molecule, which is three times larger in a liquid-like monolayer compared to a close-packed monolayer due to the uptake of the gas into the organic medium[107]. Higher residence times increase the number of collisions with the double bond and also explain why the rate of the reaction at the surface is higher than corresponding gas-phase reaction rates[6]. A further study involving the spreading and reaction at the drop surface of terminal alkenes, unsaturated organic compounds with the double bond on different positions of

the alkyl chain, and mixtures of saturated and unsaturated compounds, may be considered in order to elucidate the relative contributions of accessibility of the double bond, residence time, and nature of the monolayer substrate (solid or liquid).

Regarding the system studied by Mmereki *et al.*[64], the considerable difference in chemical nature between the compounds reacting with ozone could explain the uptake differences, since the aromaticity of anthracene could make the reaction less favorable than for a reaction with oleic acid. This is in agreement with gas-phase rate constants which show a decreased rate for the ozonolysis of aromatic compounds[6,38]. Even more important is the fact that oleic acid is forming a monolayer at the surface in which ozone can be adsorbed prior to reaction increasing the residence time of the ozone molecule at the surface. A similar effect was previously shown for a surface coated with 1-octanol which increases the uptake of ozone by the adsorbed anthracene[64].

Recently, Voss *et al.*[65] developed a similar approach to the study of the oxidation of a surface film, showing a reaction timescale comparable to ours. Furthermore, the estimation of the reaction probability for the ozonolysis of a monolayer film of OPPC spread on a Langmuir trough[43] showed a comparable value of 3×10^{-6}. On the other hand, an uptake value one order of magnitude (10^{-5}) higher was found for the processing of aqueous aerosol particles of sodium oleate mixed with Na_2SO_4 and NaCl[63]. However, since sodium oleate is soluble in water, the partitioning of this compound between the bulk and the interface likely accounts for the uptake difference. The saturation of the surface with ozone observed by McNeill *et al.*[63] at lower concentrations could be related to the low density and thickness of the oleate film, although there is no report in the

literature on the effect of these monolayer properties on the residence time of gas molecules and the accessibility of the double bond.

4.4.6. Reaction with mixtures of saturated and unsaturated phospholipids

The versatile characteristics of the main proxy used in this study, the reaction on a pendant drop, were already discussed in the initial chapters. More complex monolayers were exposed to ozone by changing various factors related to the chemical composition of the spread solution: having more units of unsaturation at the surface, compounds with longer alkyl chain length, different surface packing, and mixtures of saturated and unsaturated compounds.

Table 6 shows a summary of the results obtained. All monolayers were exposed to ozone flowing to the reaction chamber at the same rate (100 cm^3 min^{-1}) and with the same concentration (8 ppm). In addition, the reaction was carried out at two stages on the monolayer compression: at a high surface pressure where the monolayer has a high surface density but before the collapse point, and at a surface pressure value at least 10 mN m^{-1} lower. The π_0 value stands for the initial surface pressure before allowing ozone to enter the reaction chamber. The pseudo-first order rate constant k' was obtained for each sample reaction and used to characterize the reaction. Finally, the values shown in Table 6 for surface pressure and for the rate constant represent averages of three or more experiments while error values represent 2σ.

Table 6: Results of the exposure of different monolayers to ozone flowing into the reaction chamber at 100 cm^3 min^{-1} and with a concentration of 8 ppm.

Monolayer composition	π_0 (mN m^{-1})	$k' \times 10^{-3}$ (s^{-1})
Oleic acid	27	1.9 ± 0.1
	16	1.6 ± 0.8
	8	1.7 ± 0.6
DOPC	28	3.1 ± 0.6
	16	2.7 ± 1.4
Stearic acid:Oleic acid (1:1)	21	1.4 ± 0.2
	10	1.6 ± 0.4
Stearic acid:Oleic acid (2:1)	22	1.8 ± 0.6
	15	1.2 ± 0.2
DMPC:DOPC (2:1)	36	3.2 ± 0.6
	20	2.2 ± 0.1
DPPC:DOPC (2:1)	36	3.6 ± 1.6
	17	1.7 ± 0.2
DSPC:DOPC (2:1)	34	3.4 ± 0.8
	21	2.1 ± 0.4

These experiments confirmed the potential of the system developed. The kinetics of any reactive process occurring at an air-liquid interface can be studied and characterized as long as a measurable decrease of the surface pressure is observed. In

addition, the error of the rate constant determination on each sample is negligible since it is more than one order of magnitude smaller than the experimental error between experiments. Therefore, the error values shown for the rate constant represent the error provided by the reaction occurring on different samples.

From the study of the processing by ozone of organic monolayers deposited on solid substrates described in a previous section, it was found that the reaction was rather independent of the transferring surface pressure, and therefore, from the molecular surface density. In addition, those results showed that the reaction was somewhat different when comparing a pure monolayer to a mixed monolayer (the loss of hydrophobicity of DOPC monolayers was quite rapid). Differences found for the reaction on DSPC:DOPC (2:1) monolayers were attributed to the effect of surface morphology on the hydrophobic characteristics of the surface, and likewise, the measurement of contact angles. In contrast, results obtained by monitoring surface pressure changes at the air-water interface of the pendant drop seem to be free of this interference.

In general, the pseudo-first order rate obtained by exposing the pure monolayers did not show statistically significant differences to the reaction taking place on the mixtures. The error of the rate for the reaction carried out at a lower π for DOPC has a large variation that does not match common value deviations for other monolayers, likely due to a large experimental error. Moreover, similar rate values were measured for the three mixed phospholipid monolayers regardless of surface morphology or chain length difference between DOPC and the saturated organic component. It should be noted that while DMPC:DOPC forms a homogeneous mixture, DSPC:DOPC and DPPC:DOPC

show phase separation, both at the air-water interface and on solid substrates, but with different domain size and number of the condensed phase aggregates. This is well understood since ozone is evenly adsorbed throughout the monolayer, and the accommodation at the surface does not determine the probability of the reaction.

On the other hand, the differences between rates for reactions taking place at different surface densities are statistically significant for all mixed monolayers, except for the mixed monolayer of stearic acid:oleic acid (1:1). This implies a dependence of the reaction rate on the surface coverage and amount of non-reactive compounds on the surface. Since the residence time of an ozone molecule should be similar for the same monolayer, these results can only be explained as a consequence of the significance of the accessibility of the double bond for the progress of the reaction. In other words, the probability of an ozone molecule colliding with a double bond once it is adsorbed decreases at lower surface pressures, since the distance between molecules at the surface is also higher. The reaction with the (1:1) fatty acid mixed monolayer did not show this behavior likely due to a smaller difference between the two surface pressures at which the monolayer where exposed to ozone. Working at a higher surface pressure for the mixtures of stearic and oleic acid would risk having collapsed material at the surface.

The versatility of the system presented is verified by these experiments and anticipate interesting results by changing composition or working pH of the subphase. The application of the processing of surface films by using phospholipids as components of the monolayer even makes this research applicable to the study of the possible effects of ozone on the air-liquid interface of lung alveoli.

Chapter 5

CONCLUSIONS

5.1. Study of model systems for the processing of organic monolayers

The focus of this research project was to find a suitable model for the processing of atmospheric organic aerosols, mainly for those described by the proposed inverted micelle model. The purpose was to follow the reaction with ozone through the changes in the surface properties of the monolayer. While atomic force microscopy revealed small changes in mixed monolayers of phospholipids after reaction with ozone, those changes were not sufficient for a quantitative description of the reaction. On the other hand, the variation of layer thickness of the processed monolayers measured by ellipsometry was not appreciable either. Possible rearrangements of the monolayer and reaction products remaining at the surface prevent the observation of quantifiable variations when using both techniques.

The measurement of the contact angle of a water drop placed on monolayers transferred to mica and exposed to ozone for different times enabled the variation of the hydrophobic properties of the surface to be followed. The loss of hydrophobicity showed a trend for all analyzed monolayers that was related to the rate of the reaction taking place at the surface. However, it was also found that the contact angle was highly

dependant on the morphology of the deposited monolayer, for instance, because of monolayer transfer or phase coexistence. The presence of phase domains was shown to increase the hydrophobic character of the surface when compared to a homogeneous surface. In general, the estimation of kinetic parameters from the results of these measurements is feasible but highly influenced by monolayer characteristics and experimental errors. Nevertheless, the processing of the monolayers deposited on solid substrates provides valuable data on hydrophobicity changes due to reaction, which is directly related to cloud nucleation capabilities and water uptake, mainly for complex mixed organic films.

Finally, the exposure to ozone of a monolayer spread at the air-water interface of a pendant drop demonstrated to be a novel model system for the study of the gas phase-aerosol particle interaction, which permitted the analysis of the kinetics of interfacial reactions and their effect on surface properties. The variable measured, the surface pressure of the interface, was used for the calculation of a surface-specific second order rate constant for the reaction, which led to the estimation of the reactive uptake of ozone by an oleic acid monolayer. This was found to be $(2.6 \pm 0.1) \times 10^{-6}$, which is a value comparable to those previously reported for the reactive uptake. This result highlighted the importance of taking into account the contribution of the accessibility of the unit of unsaturation to the gas species after collision with the surface as well as the residence time of the ozone molecule on the organic medium. The proxy studied made possible the analysis of the kinetics of a system in which it is important to monitor only the surface reaction as is in the case of the proposed inverted micelle model for organic liquid

aerosols, and any situation of surface-adsorbed organic species reacting with an atmospheric oxidant. The versatility of this proxy was confirmed by the measurement and comparison of the pseudo-first order rate constants for the ozonolysis on pure and mixed monolayers of known phospholipids. In addition, the rates presented in this section for the surface reactions at the air-water interface are, to our knowledge, the first results reported in the literature for mixed monolayers, which corroborates the novelty of the system developed.

In summary, a system was developed for the analysis and real-time monitoring of heterogeneous chemical reactions involving a gas phase species and a condensed phase. The instrumentation used saves laboratory costs as small amounts of chemicals are utilized. A major benefit of this approach is that it ensures that measured kinetics is related exclusively to processes taking place at the surface. In addition, the proposed setup permits the experimental conditions to be easily changed, and therefore makes the system applicable to a wide range of research fields.

5.2. Future work

The model system developed here to analyze and follow reactions occurring at the air-liquid interface can be applied to wider research aims and more complex situations. Since the initial approach was to mimic inverted-micelle like aerosols, several steps can be taken to approximate the characteristics of the real matrix. This could be achieved by changing the subphase over which the monolayer is spread, for example, by choosing NaCl or Na_2SO_4 solutions at concentrations reported in field experiment determinations.

In addition, an atmospheric aerosol is normally composed of several different compounds, which could be simulated by spreading binary or tertiary mixtures of saturated and unsaturated fatty acids, alkenes, or phospholipids. Experiments should be designed as well where the position of the unsaturation is varied, given the importance of the accessibility of the double bond to the reaction rate.

Fatty acids could also be combined with compounds having complex structures that represent organic compounds of anthropogenic origin typically found in field experiments, such as polycyclic aromatic hydrocarbons (PAH, i.e. benzo[a]pyrene, anthracene, phenanthrene). Furthermore, it would be possible to study the processing of these pollutants not only when co-spreading with a monolayer but also by partitioning to the surface from the liquid bulk. The potential influence on the outcome of the reaction of all applied changes would be identified. Finally, the measurement and control of experimental conditions surrounding the drop, such as humidity, temperature, and ozone concentration, should be also improved.

On the other hand, the results found for the ozonolysis of mixed monolayers showed the need for a deep examination of the influence that monolayer density and compression have in the residence time of ozone and the saturation of the surface as predicted by the Langmuir-Hinshelwood mechanism. This research should be accompanied by analysis of water uptake before and after processing of the organic coating film, and at different levels of monolayer compression. The instruments utilized allow experiments to be carried out without controlling area and volume. It has not yet been tested if appreciable measurements of water uptake could be achieved. An ideal

system would be one in which the current setup is coupled to any technique that could permit a characterization of the reaction products at the surface or in the bulk of the drop.

To conclude, the application of the same system to the study of the harmful effect of ozone to lung surfactants is promising. The processing of mixed monolayers systems of typical pulmonary lipids and proteins by pollutants, such as ozone or tobacco smoke, could be easily studied. This would discover any adverse effects on monolayer surface activity and rheology, which would reflect the capability of the pulmonary system to function after exposure to severe pollution.

REFERENCES

1. Seinfeld, J. H.; Pandis, S. N. *Atmospheric Chemistry & Physics: From Air Pollution to Climate Change*, 2nd edition ed.; John Wiley & Sons: New York, 2006.
2. Seinfeld, J. H. *AICHE Journal* **2004**, *50*, 1096-1108.
3. Reid, J. P.; Sayer, R. M. *Science Progress* **2002**, *85*, 263-296.
4. Poschl, U. *Angewandte Chemie - International Edition* **2005**, *44*, 7520-7540.
5. Kanakidou, M.; Seinfeld, J. H.; Pandis, S. N.; Barnes, I.; Dentener, F. J.; Facchini, M. C.; Van Dingenen, R.; Ervens, B.; Nenes, A.; Nielsen, C. J.; Swietlicki, E.; Putaud, J. P.; Balkanski, Y.; Fuzzi, S.; Horth, J.; Moortgat, G. K.; Winterhalter, R.; Myhre, C. E. L.; Tsigaridis, K.; Vignati, E.; Stephanou, E. G.; Wilson, J. *Atmospheric Chemistry and Physics* **2005**, *5*, 1053-1123.
6. Finlayson-Pitts, B. J.; Pitts, J. N. J. *Chemistry of the Upper and Lower Atmosphere*; Academic Press: San Diego, 1999.
7. Donaldson, D. J.; Tervahattu, H.; Tuck, A. F.; Vaida, V. *Origins of Life and Evolution of the Biosphere* **2004**, *34*, 57-67.

8. Ellison, G. B.; Tuck, A. F.; Vaida, V. *Journal of Geophysical Research, [Atmospheres]* **1999**, *104*, 11633-11641.

9. Fuzzi, S.; Andreae, M. O.; Huebert, B. J.; Kulmala, M.; Bond, T. C.; Boy, M.; Doherty, S. J.; Guenther, A.; Kanakidou, M.; Kawamura, K.; Kerminen, V. M.; Lohmann, U.; Russell, L. M.; Poschl, U. *Atmospheric Chemistry and Physics* **2006**, *6*, 2017-2038.

10. Rudich, Y. *Chemical Reviews* **2003**, *103*, 5097-5124.

11. Zahardis, J.; Petrucci, G. A. *Atmospheric Chemistry and Physics* **2007**, *7*, 1237-1274.

12. Donaldson, D. J.; Vaida, V. *Chemical Reviews* **2006**, *106*, 1445-1461.

13. Ramanathan, V.; Crutzen, P. J.; Kiehl, J. T.; Rosenfeld, D. *Science (Washington, D. C.)* **2001**, *294*, 2119-2124.

14. Middlebrook, A. M.; Murphy, D. M.; Thomson, D. S. *Journal of Geophysical Research* **1998**, *103*, 16475-16484.

15. Mochida, M.; Kitamori, Y.; Kawamura, K.; Nojiri, Y.; Suzuki, K. *Journal of Geophysical Research, [Atmospheres]* **2002**, *107*, AAC1/1-AAC1/10.

16. Husar, R. B.; Shu, W. R. *Journal of Applied Meteorology* **1975**, *14*, 1558-1565.

17. Tervahattu, H.; Juhanoja, J.; Kupiainen, K. *Journal of Geophysical Research, [Atmospheres]* **2002**, *107*, ACH18/11-ACH18/17.

18. Tervahattu, H.; Hartonen, K.; Kerminen, V.-M.; Kupiainen, K.; Aarnio, P.; Koskentalo, T.; Tuck, A. F.; Vaida, V. *Journal of Geophysical Research, [Atmospheres]* **2002**, *107*, AAC 1/1-AAC 1/9.

19. Tervahattu, H.; Juhanoja, J.; Vaida, V.; Tuck, A. F.; Niemi, J. V.; Kupiainen, K.; Kulmala, M.; Vehkamaki, H. *Journal of Geophysical Research, [Atmospheres]* **2005**, *110*, D06207/06201-D06207/06209.

20. Seinfeld, J. H.; Pandis, S. N. *Atmospheric Chemistry & Physics: From Air Pollution to Climate Change*; John Wiley & Sons: New York, 1998.

21. Rogge, W. F.; Hildemann, L. M.; Mazurek, M. A.; Cass, G. R.; Simonelt, B. R. T. *Environmental Science and Technology* **1991**, *25*, 1112-1125.

22. Sun, J. M.; Ariya, P. A. *Atmospheric Environment* **2006**, *40*, 795-820.

23. McFiggans, G.; Artaxo, P.; Baltensperger, U.; Coe, H.; Facchini, M. C.; Feingold, G.; Fuzzi, S.; Gysel, M.; Laaksonen, A.; Lohmann, U.; Mentel, T. F.; Murphy, D. M.; O'Dowd, C. D.; Snider, J. R.; Weingartner, E. *Atmospheric Chemistry and Physics* **2006**, *6*, 2593-2649.

24. Cruz, C. N.; Pandis, S. N. *Journal of Geophysical Research, [Atmospheres]* **1998**, *103*, 13111-13123.

25. Saxena, P.; Hildemann, L. M.; McMurry, P. H.; Seinfeld, J. H. *Journal of Geophysical Research* **1995**, *100*, 18755-18770.

26. Decesari, S.; Facchini, M. C.; Fuzzi, S.; McFiggans, G. B.; Coe, H.; Bower, K. N. *Atmospheric Environment* **2005**, *39*, 211-222.

27. Andreae, M. O.; Crutzen, P. J. *Science (Washington, D. C.)* **1997**, *276*, 1052-1058.

28. Jaeglé, L.; Jacob, D. J.; Brune, W. H.; Wennberg, P. O. *Atmospheric Environment* **2000**, *35*, 469-489.

29. Russell, L. M.; Maria, S. F.; Myneni, S. C. B. *Geophysical Research Letters* **2002**, *29*.

30. Facchini, M. C.; Decesari, S.; Mirceaa, M.; Fuzzi, S.; Loglio, G. *Atmospheric Environment* **2000**, *34*, 4853-4857.

31. Posfai, M.; Xu, H. F.; Anderson, J. R.; Buseck, P. R. *Geophysical Research Letters* **1998**, *25*, 1907-1910.

32. Simoneit, B. R. T.; Kobayashi, M.; Mochida, M.; Kawamura, K.; Lee, M.; Lim, H. J.; Turpin, B. J.; Komazaki, Y. *Journal of Geophysical Research* **2004**, *109*.

33. Mochida, M.; Kawamura, K.; Umemoto, N.; Kobayashi, M.; Matsunaga, S.; Lim, H. J.; Turpin, B. J.; Bates, T. S.; Simoneit, B. R. T. *Journal of Geophysical Research* **2003**, *108*.

34. Rogge, W. F.; Hildemann, L. M.; Mazurek, M. A.; Cass, G. R.; Simoneit, B. R. T. *Environmental Science and Technology* **1993**, *27*, 2700-2711.

35. Rogge, W. F.; Mazurek, M. A.; Hildemann, L. M.; Cass, G. R.; Simoneit, B. R. T. *Atmospheric Environment* **1993**, *27*, 1309-1330.

36. Rogge, W. F.; Hildemann, L. M.; Mazurek, M. A.; Cass, G. R.; Simoneit, B. R. T. *Environmental Science and Technology* **1998**, *32*, 13-22.

37. Criegee, R. *Angewandte Chemie* **1975**, *87*, 765-771.

38. Atkinson, R.; Carter, W. P. L. *Chemical Reviews (Washington, DC, United States)* **1984**, *84*, 437-470.

39. Dubowski, Y.; Vieceli, J.; Tobias, D. J.; Gomez, A.; Lin, A.; Nizkorodov, S. A.; McIntire, T. M.; Finlayson-Pitts, B. J. *Journal of Physical Chemistry A* **2004**, *108*, 10473-10485.

40. Thomas, E. R.; Frost, G. J.; Rudich, Y. *Journal of Geophysical Research, [Atmospheres]* **2001**, *106*, 3045-3056.

41. Moise, T.; Rudich, Y. *Journal of Geophysical Research, [Atmospheres]* **2000**, *105*, 14667-14676.

42. Moise, T.; Rudich, Y. *Journal of Physical Chemistry A* **2002**, *106*, 6469-6476.

43. Wadia, Y.; Tobias, D. J.; Stafford, R.; Finlayson-Pitts, B. J. *Langmuir* **2000**, *16*, 9321-9330.

44. De Gouw, J. A.; Lovejoy, E. R. *Geophysical Research Letters* **1998**, *25*, 931-934.

45. Hearn, J. D.; Lovett, A. J.; Smith, G. D. *Physical Chemistry Chemical Physics* **2005**, *7*, 501-511.

46. King, M. D.; Thompson, K. C.; Ward, A. D. *Journal of the American Chemical Society* **2004**, *126*, 16710-16711.

47. Smith, G. D.; Woods, E., III; DeForest, C. L.; Baer, T.; Miller, R. E. *Journal of Physical Chemistry A* **2002**, *106*, 8085-8095.

48. Ziemann, P. J. *Faraday Discussions* **2005**, *130*, 469-490.

49. Morris, J. W.; Davidovits, P.; Jayne, J. T.; Jimenez, J. L.; Shi, Q.; Kolb, C. E.; Worsnop, D. R.; Barney, W. S.; Cass, G. *Geophysical Research Letters* **2002**, *29*, 71/71-71/74.

50. Chughtai, A. R.; Jassim, J. A.; Peterson, J. H.; Stedman, D. H.; Smith, D. M. *Aerosol Science and Technology* **1991**, *15*, 112-126.

51. Hung, H. M.; Katrib, Y.; Martin, S. T. *Journal of Physical Chemistry A* **2005**, *109*, 4517-4530.

52. Decesari, S.; Facchini, M. C.; Matta, E.; Mircea, M.; Fuzzi, S.; Chughtai, A. R.; Smith, D. M. *Atmospheric Environment* **2002**, *36*, 1827-1832.

53. Demou, E.; Visram, H.; Donaldson, D. J.; Makar, P. A. *Atmospheric Environment* **2003**, *37*, 3529-3537.

54. Worsnop, D. R.; Morris, J. W.; Shi, Q.; Davidovits, P.; Kolb, C. E. *Geophysical Research Letters* **2002**, *29*, 57/51-57/54.

55. Davidovits, P.; Kolb, C. E.; Williams, L. R.; Jayne, J. T.; Worsnop, D. R. *Chemical Reviews* **2006**, *106*, 1323-1354.

56. Srisankar, E. V.; Patterson, L. K. *Archives of Environmental Health* **1979**, *34*, 346-349.

57. Lai, C. C.; Yang, S. H.; Finlayson-Pitts, B. J. *Langmuir* **1994**, *10*, 4637-4644.

58. Thornberry, T.; Abbatt, J. P. D. *Physical Chemistry Chemical Physics* **2004**, *6*, 84-93.

59. Knopf, D. A.; Anthony, L. M.; Bertram, A. K. *Journal of Physical Chemistry A* **2005**, *109*, 5579-5589.

60. Eliason, T. L.; Aloisio, S.; Donaldson, D. J.; Cziczo, D. J.; Vaida, V. *Atmospheric Environment* **2003**, *37*, 2207-2219.

61. Katrib, Y.; Martin, S. T.; Hung, H. M.; Rudich, Y.; Zhang, H. Z.; Slowik, J. G.; Davidovits, P.; Jayne, J. T.; Worsnop, D. R. *Journal of Physical Chemistry A* **2004**, *108*, 6686-6695.

62. Katrib, Y.; Biskos, G.; Buseck, P. R.; Davidovits, P.; Jayne, J. T.; Mochida, M.; Wise, M. E.; Worsnop, D. R.; Martin, S. T. *Journal of Physical Chemistry A* **2005**, *109*, 10910-10919.

63. McNeill, V. F.; Wolfe, G. M.; Thornton, J. A. *Journal of Physical Chemistry A* **2007**, *111*, 1073-1083.

64. Mmereki, B. T.; Donaldson, D. J. *Journal of Physical Chemistry A* **2003**, *107*, 11038-11042.

65. Voss, L. F.; Bazerbashi, M. F.; Beekman, C. P.; Hadad, C. M.; Allen, H. C. *Journal of Geophysical Research, [Atmospheres]* **2007**, *112*, 1-9.

66. Voss, L. F.; Hadad, C. M.; Allen, H. C. *Journal of Physical Chemistry B* **2006**, *110*, 19487-19490.

67. Kahan, T. F.; Kwamena, N. O. A.; Donaldson, D. J. *Atmospheric Environment* **2006**, *40*, 3448-3459.

68. Kwamena, N. O. A.; Earp, M. E.; Young, C. J.; Abbatt, J. P. D. *Journal of Physical Chemistry A* **2006**, *110*, 3638-3646.

69. Poschl, U.; Letzel, T.; Schauer, C.; Niessner, R. *Journal of Physical Chemistry A* **2001**, *105*, 4029-4041.

70. Pockels, A. *Nature* **1891**, *43*, 437.

71. Langmuir, I. *Journal of the American Chemical Society* **1917**, *39*, 1848-1906.

72. Adamson, A. W.; Gast, A. P. *Physical Chemistry of Surfaces*; John Wiley and Sons: New York, 1997.

73. Kaganer, V. M.; Mohwald, H.; Dutta, P. *Rev. Mod. Phys.* **1999**, *71*, 779-819.

74. Giessibl, F. J. *Reviews of Modern Physics* **2003**, *75*, 949-983.

75. Dufrene, Y. F.; Lee, G. U. *Biochimica et Biophysica Acta* **2000**, *1509*, 14-41.

76. Stark, M.; Moller, C.; Muller, D. J.; Guckenberger, R. *Biophysical Journal* **2001**, *80*, 3009-3018.

77. Garcia, R.; Perez, R. *Surface Science Reports* **2002**, *47*, 197-301.

78. Babcock, K. L.; Prater, C. B. Phase imaging: beyond topography; Veeco Instruments Inc.: Santa Barbara, CA, 2004.

79. Cevc, G. *Phospholipid Handbook*; Marcel Dekker: New York, 1993.

80. Kwok, D. Y.; Vollhardt, D.; Miller, R.; Li, D.; Neumann, A. W. *Colloids and Surfaces, A: Physicochemical and Engineering Aspects* **1994**, *88*, 51-58.

81. Chen, P.; Mak, C.; Susnar, S. S.; Neumann, A. W. *Journal of Physical Chemistry B* **1998**, *102*, 2511-2518.

82. Hoorfar, M.; Neumann, A. W. *Journal of Adhesion* **2004**, *80*, 727-743.

83. González-Labrada, E.; Schmidt, R.; DeWolf, C. E. *Chemical Communications* **2006**, 2471-2473.

84. Myers, D. *Surfaces, Interfaces, and Colloids: Principles and Applications*; Wiley-VCH: New York, 1999.

85. Iimura, K.; Yamauchi, Y.; Tsuchiya, Y.; Kato, T. *Langmuir* **2001**, *17*, 4602-4609.

86. Kajiyama, T.; Oishi, Y. *Studies in Interface Science* **1996**, *4*, 1-38.

87. Seoane, R.; Dynarowicz-tstka, P.; Minones, J.; Rey-Gomez-Serranillos, I. *Colloid and Polymer Science* **2001**, *279*, 562-570.

88. Vollhardt, D. *Journal of Physical Chemistry C* **2007**, *111*, 6805-6812.

89. Asad, A.; Mmereki, B. T.; Donaldson, D. J. *Atmospheric Chemistry and Physics* **2004**, *4*, 4019–4038.

90. Nie, H. Y.; Walzak, M. J.; McIntyre, N. S. *Journal of Physical Chemistry B* **2006**, *110*, 21101-21108.

91. Ulman, A. *Chemical Reviews* **1996**, *96*, 1533-1554.

92. DeWolf, C.; Leporatti, S.; Kirsch, C.; Klinger, R.; Brezesinski, G. *Chem. Phys. Lipids* **1999**, *97*, 129-138.

93. Dufrene, Y. F.; Barger, W. R.; Green, J. B. D.; Lee, G. U. *Langmuir* **1997**, *13*, 4779-4784.

94. Nag, K.; Keough, K. M. W. *Biophysical Journal* **1993**, *65*, 1019-1026.

95. Moraille, P.; Badia, A. *Langmuir* **2002**, *18*, 4414-4419.

96. Hui, S. W.; Viswanathan, R.; Zasadzinski, J. A.; Israelachvili, J. N. *Biophysical Journal* **1995**, *68*, 171-178.

97. McIntire, T. M.; Lea, A. S.; Gaspar, D. J.; Jaitly, N.; Dubowski, Y.; Li, Q. Q.; Finlayson-Pitts, B. J. *Physical Chemistry Chemical Physics* **2005**, *7*, 3605-3609.

98. Callies, M.; Quere, D. *Soft Matter* **2005**, *1*, 55-61.

99. Furstner, R.; Barthlott, W.; Neinhuis, C.; Walzel, P. *Langmuir* **2005**, *21*, 956-961.

100. Doerfler, H. D.; Rettig, W. *Colloid and Polymer Science* **1980**, *258*, 839-848.

101. Wustneck, R.; Wustneck, N.; Moser, B.; Karageorgieva, V.; Pison, U. *Langmuir* **2002**, *18*, 1119-1124.

102. Jyoti, A.; Prokop, R. M.; Neumann, A. W. *Colloids and Surfaces, B: Biointerfaces* **1997**, *8*, 115-124.

103. Wege, H. A.; Holgado-Terriza, J. A.; Galvez-Ruiz, M. J.; Cabrerizo-Vilchez, M. A. *Colloids and Surfaces, B: Biointerfaces* **1999**, *12*, 339-349.

104. Hansen, F. K.; Myrvold, R. *Journal of Colloid and Interface Science* **1995**, *176*, 408-417.

105. Barnes, G. T.; Feher, A. I. *Journal of Colloid and Interface Science* **1980**, *75*, 584-589.

106. Erbil, H. Y.; Dogan, M. *Langmuir* **2000**, *16*, 9267-9273.

107. Vieceli, J.; Ma, O. L.; Tobias, D. J. *Journal of Physical Chemistry A* **2004**, *108*, 5806-5814.

108. Atkins, P. W.; De Paula, J. *Physical Chemistry*, 8th ed.; Oxford University Press: Oxford, 2002.

109. Ivanov, A. V.; Trakhtenberg, S.; Bertram, A. K.; Gershenzon, Y. M.; Molina, M. J. *Journal of Physical Chemistry A* **2007**, *111*, 1632-1637.

110. Hegeler, F.; Akiyama, H. *IEEE Transactions on Plasma Science* **1997**, *25*, 1158-1165.

111. Poschl, U.; Rudich, Y.; Ammann, M. *Atmospheric Chemistry and Physics Discussions* **2005**, *5*, 2111-2191.